LBL-24752
NDC-1

NAGRA-DOE
COOPERATIVE
PROJECT REPORT

Determination of Fracture Inflow Parameters with a Borehole Fluid Conductivity Logging Method

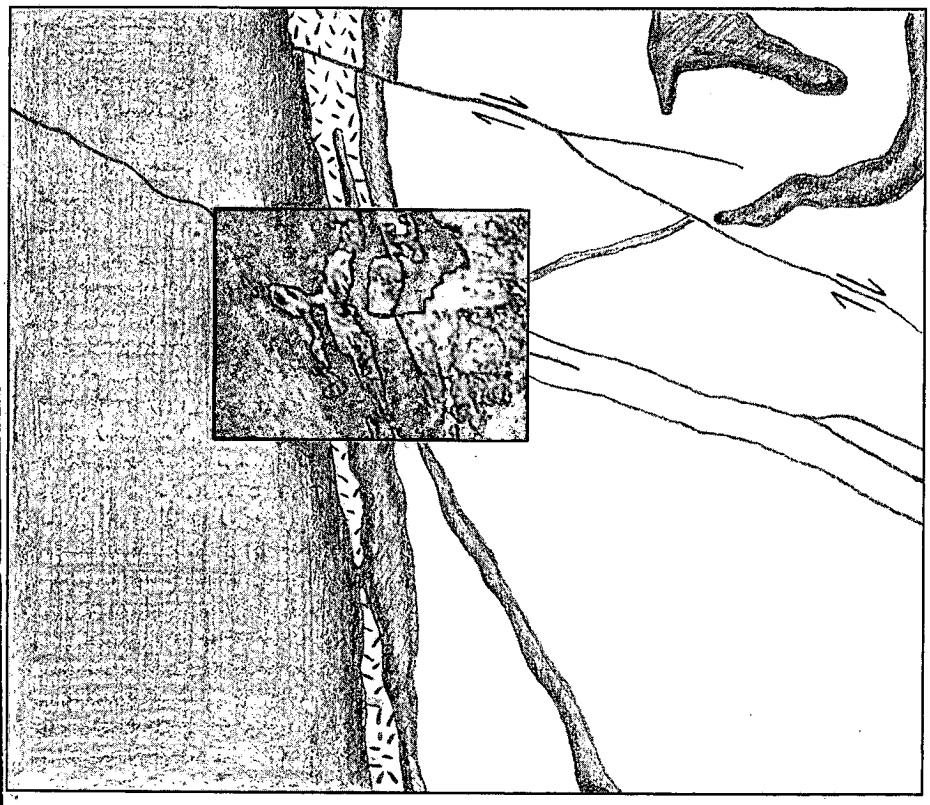

Chin-Fu Tsang, Peter Hufschmied, and Frank V. Hale

September 1989

LOAN COPY
Circulates
for 2 weeks
Bldg. 50 Library.
Copy 2
LBL-24752

Swiss National Cooperative for
the Storage of Nuclear Waste
NAGRA
CH-5401 Baden, Switzerland

Earth Sciences Division
Lawrence Berkeley Laboratory
University of California
Berkeley, California 94720, USA

Prepared for the U.S. Department of Energy under Contract DE-AC03-76SF00098

DISCLAIMER

This document was prepared as an account of work sponsored by the United States Government. While this document is believed to contain correct information, neither the United States Government nor any agency thereof, nor the Regents of the University of California, nor any of their employees, makes any warranty, express or implied, or assumes any legal responsibility for the accuracy, completeness, or usefulness of any information, apparatus, product, or process disclosed, or represents that its use would not infringe privately owned rights. Reference herein to any specific commercial product, process, or service by its trade name, trademark, manufacturer, or otherwise, does not necessarily constitute or imply its endorsement, recommendation, or favoring by the United States Government or any agency thereof, or the Regents of the University of California. The views and opinions of authors expressed herein do not necessarily state or reflect those of the United States Government or any agency thereof or the Regents of the University of California.

LBL-24752
NDC-1

Determination of Fracture Inflow Parameters with a Borehole Fluid Conductivity Logging Method

Chin-Fu Tsang and Frank V. Hale

Earth Sciences Division
Lawrence Berkeley Laboratory
University of California
Berkeley, California 94720

Peter Hufschmied

Swiss National Cooperative for the Storage of Nuclear Waste
Baden, Switzerland

September 1989

Also published in
Water Resources Research,
Vol. 26, No. 4, pp. 561–578, 1990

This work was supported by the Manager, Chicago Operations, Repository Technology Program, Repository Technology and Transportation Division, of the U.S. Department of Energy under Contract No. DE-AC03-76SF00098 and by the Swiss National Cooperative for the Storage of Nuclear Waste (NAGRA).

Preface

This report is one of a series documenting the results of the Nagra-DOE Cooperative (NDC-I) research program in which the cooperating scientists explore the geological, geophysical, hydrological, geochemical, and structural effects anticipated from the use of a rock mass as a geologic repository for nuclear waste. This program was sponsored by the U. S. Department of Energy (DOE) through the Lawrence Berkeley Laboratory (LBL) and the Swiss Nationale Genossenschaft für die Lagerung radioaktiver Abfälla (Nagra) and concluded in September 1989. The principal investigators are Jane C. S. Long, Ernest L. Majer, Karsten Pruess, Kenzi Karasaki, Chalon Carnahan and Chin-Fu Tsang for LBL and Piet Zuidema, Peter Blümling, Peter Hufschmied and Stratis Vomvoris for Nagra. Other participants will appear as authors of the individual reports. Technical reports in this series are listed below.

1. Determination of Fracture Inflow Parameters with a Borehole Fluid Conductivity Logging Method by Chin-Fu Tsang, Peter Hufschmied, and Frank V. Hale (NDC-1, LBL-24752).
2. A Code to Compute Borehole Fluid Conductivity Profiles with Multiple Feed Points by Frank V. Hale and Chin-Fu Tsang (NDC-2, LBL-24928; also NTB 88-21).
3. Numerical Simulation of Alteration of Sodium Bentonite by Diffusion of Ionic Groundwater Components by Janet S. Jacobsen and Chalon L. Carnahan (NDC-3, LBL-24494).
4. P-Wave Imaging of the FRI and BK Zones at the Grimsel Rock Laboratory by Ernest L. Majer, John E. Peterson Jr., Peter Blümling, and Gerd Sattel (NDC-4, LBL-28807).
5. Numerical Modeling of Gas Migration at a Proposed Repository for Low and Intermediate Level Nuclear Wastes at Oberbauenstock, Switzerland by Karsten Pruess (NDC-5, LBL-25413).
6. Analysis of Well Test Data from Selected Intervals in Leuggern Deep Borehole — Verification and Application of PTST Method by Kenzi Karasaki (NDC-6, LBL-27914).
7. Shear Wave Experiments at the U. S. Site at the Grimsel Laboratory by Ernest L. Majer, John E. Peterson Jr., Peter Blümling, and Gerd Sattel (NDC-7 LBL-28808).
8. The Application of Moment Methods to the Analysis of Fluid Electrical Conductivity Logs in Boreholes by Simon Loew, Chin-Fu Tsang, Frank V. Hale, and Peter Hufschmied (NDC-8, LBL-28809).
9. Numerical Simulation of Cesium and Strontium Migration through Sodium Bentonite Altered by Cation Exchange with Groundwater Components by Janet S. Jacobsen and Chalon L. Carnahan (NDC-9, LBL-26395).
10. Theory and Calculation of Water Distribution in Bentonite in a Thermal Field by Chalon L. Carnahan (NDC-10, LBL-26058).
11. Prematurely Terminated Slug Tests by Kenzi Karasaki (NDC-11, LBL-27528).
12. Hydrologic Characterization of Fractured Rocks — An Interdisciplinary Methodology by Jane C. S. Long, Ernest L. Majer, Stephen J. Martel, Kenzi Karasaki, John E. Peterson Jr., Amy Davey, and Kevin Hestir, (NDC-12, LBL-27863).
13. Exploratory Simulations of Multiphase Effects in Gas Injection and Ventilation Tests in an Underground Rock Laboratory by Stefan Finsterle, Erika Schlueter, and Karsten Pruess (NDC-13, LBL-28810).
14. Joint Seismic, Hydrogeological, and Geomechanical Investigations of a Fracture Zone in the Grimsel Rock Laboratory, Switzerland by Ernest L. Majer, Larry R. Myer, John E. Peterson Jr., Kenzi Karasaki, Jane C. S. Long, Stephen J. Martel, Peter Blümling, and Stratis Vomvoris (NDC-14, LBL-27913).
15. Analysis of Hydraulic Data from the MI Fracture Zone at the Grimsel Rock Laboratory, Switzerland by Amy Davey, Kenzi Karasaki, Jane C.S. Long, Martin Landsfeld, Antoine Mensch, and Stephen J. Martel (NDC-15, LBL-27864).
16. Use of Integrated Geologic and Geophysical Information for Characterizing the Structure of Fracture Systems at the US/BK Site, Grimsel Laboratory, Switzerland by Stephen J. Martel and John E. Peterson Jr. (NDC-16, LBL-27912).

Table of Contents

List of Figures vii
List of Tables ix
Abstract xi
Nomenclature xiii
Acknowledgements xv

Introduction 1

Fluid Conductivity Logging Procedure 2

Analytical Considerations 8

Numerical Method 14

Application to a Synthetic Data Set 17

Field Experiment and Data Analysis 20

Estimation and Transmissivities from the Results of Fluid Conductivity Logging 33

Comparison of Transmissivities Derived from Fluid Conductivity Logging and Conventional Hydraulic Testing 39

Comparison with Results of Hydrochemical Sampling 41

Conclusions and Discussion 44

References 47

List of Figures

		Page
Figure 1.	Schematic picture of a well bore with three inflow points and a well bore flow rate w from below.	4
Figure 2.	Schematic picture of salinity curves from three inflow points in a well bore at three early times. Higher curves correspond to later times.	4
Figure 3.	Schematic picture of salinity curves at a large time, assuming very small diffusion effects.	5
Figure 4.	Schematic picture of salinity concentration curves at the very large time limit, assuming very small diffusion effects.	5
Figure 5.	Schematic picture of salinity concentration curves from early to later times, assuming one of the three inflow points begins much earlier than the other two. Lower curves correspond to earlier times.	6
Figure 6.	Schematic diagram of a well bore with several inflow points, each with a flow rate q_i, concentration C_i, and position x_i. The total flow rate out of the well is Q, the initial salinity is C_0, and the inflow at the bottom of the well is w. Positions are indicated assuming the origin at the surface and increasing with depth.	10
Figure 7.	Numerical results for one inflow point from early to late times.	15
Figure 8.	Numerical results for one inflow point at flow rate q for three values of well bore flow rate from below: w = 0, w = q/3 and w = q.	15
Figure 9.	Numerical results for one inflow point and w = 0.	16
Figure 10.	Numerical results for two inflow points.	16
Figure 11.	Synthetic results at 0.5, 144 and 600 hours (from lower curve to highest curve respectively).	19

Figure 12.	Results of synthetic initial estimate for two times, 0.5 and 600 hours, using 96-hour data.	19
Figure 13.	Results after adjusting parameters for the synthetic case. Results for 0.5 and 600 hours are shown.	21
Figure 14.	Sensitivity to K variation.	21
Figure 15.	Effect of increasing q while maintaining constant qC.	22
Figure 16.	Effect of decreasing C and qC.	22
Figure 17.	Effect of decreasing q and qC.	24
Figure 18.	Map of Northern Switzerland, with the location of the Leuggern borehole.	24
Figure 19.	Geological formation intersected by the Leuggern borehole, and other borehole characteristics.	25
Figure 20.	Field fluid conductivity log data from Thury (1986) for the 770-1000 m section of a 1690-m borehole.	27
Figure 21.	Field fluid conductivity log data from Thury (1986) for the full logged 770-1610 m section of a 1690-m borehole.	27
Figure 22.	Normalized fluid conductivity log data.	29
Figure 23.	Area versus time plots for all nine inflow points.	29
Figure 24.	Initial fit to field data.	31
Figure 25.	Final fit to field data.	32

List of Tables

		Page
Table 1.	Parameter estimates for synthetic case.	18
Table 2.	Parameters used in sensitivity analysis: Base case.	23
Table 3.	Data from $\int\sigma$ (x,t) dx vs t curves.	30
Table 4.	Parameters used in initial match of field data.	30
Table 5.	Parameters used in final match of field data.	33
Table 6.	Comparison of transmissivities derived from fluid logging and conventional packer hydraulic testing.	37
Table 7.	Transmissivities derived from fluid conductivity logging for test cases A through E. Base case is C.	38
Table 8.	Chemical composition and electric conductivity of formation water from four test sections.	42
Table 9.	Comparison of formation water electric conductivity (at 20°C equivalent) derived from fluid conductivity logging and from water sampling.	44

Abstract

There is much current interest in determining the flow characteristics of fractures intersecting a well bore in order to provide data for use in estimating the hydrologic behavior of fractured rocks. Inflow rates from these fractures into the well bore are usually very low. Moreover, in most cases, only a few percent of the fractures identified by core inspection and geophysical logging actually conduct water, the rest being closed, clogged, or isolated from the water flow system. A new procedure is proposed and a corresponding method of analysis developed to locate water-conducting fractures and obtain fracture inflow rates by means of a time sequence of electric conductivity logs of the borehole fluid. The physical basis of the analysis method is discussed, and the procedure is applied to an existing set of data, which shows initiation and growth of nine conductivity peaks in a 900-m section of a 1690-m borehole, corresponding to nine water-conducting fractures intersecting the borehole. By applying our analysis to these nine peaks, the flow rates and the salinity of the water from these fractures are determined. These results are used with other information to obtain transmissivities of the nine fractures, which are validated against independent hydraulic measurements by packer tests. The salinities measured in fluids from the fractures are also validated against salinity values obtained by chemical sampling of fluids from different depths of the borehole. The applicability of this technique is discussed in the context of a borehole-testing program.

Nomenclature

a	rock compressibility, $m \cdot s^2/kg$
b	formation fluid compressibility, $m \cdot s^2/kg$
C	fluid electrolyte concentration, kg/m^3
C_i	electrolyte concentration of fluid flowing from inflow i to the borehole, kg/m^3
$C_{max,i}$	maximum concentration observed immediately downstream of inflow i, kg/m^3
C_o	electrolyte concentration of fluid flowing from bottom of well, kg/m^3
$C(L,t)$	electrolyte concentration of fluid at depth L at time t, kg/m^3
$\bar{C}_L(t)$	average concentration in the borehole section from L_o to L at time t, kg/m^3
G	mass source or sink, $kg \cdot s/m^3$
g	gravity acceleration, m/s^2
$H(t-t_i)$	Heaviside step function, 0 for $t \leq t_i$ and 1 for $t > t_i$
h	hydraulic head, m
h_i	head opposite inflow zone i, m
h_o	initial uniform head, m
$h(r,t)$	head at radial distance r at time t, m
K	dispersion coefficient, m^2/s
L	a depth in the section of interest, m
L_o	a reference depth near the bottom of the well, m
m	thickness of flow zone, m
n	porosity, dimensionless
Q	flow rate out of a borehole section, m^3/s or L/min
Q_L	flow rate at depth L out of the section from L_o to L, m^3/s
Q_w	discharge from well, m^3/s or L/min
q_i	flow rate from inflow i to the borehole, m^3/s or L/min
$q_i C_i$	mass flux from inflow i to the borehole, kg/s
r_w	wellbore radius, m

r	radial distance from well, m
S	storativity, dimensionless
S_s	specific storativity, m^{-1}
S_{s_i}	specific storativity of aquifer i, m^{-1}
$s(r,t)$	drawdown at radial distance r and time t, m
T	transmissivity, m^2/s
t	time, s or hr
t_i	time at which inflow i begins flowing with concentration C_i, s or hr
u	dimensionless argument of well function, $r^2S/4Tt$
v	fluid linear velocity, m/s
$W(u)$	well function
w	flow rate at bottom of well, m^3/s or L/min
wC_o	max flux from bottom of well, kg/s
x	depth, m
x_i	depth of inflow i, m
α	factor relating concentration and conductivity, 1870 $(\mu S/cm)\cdot(m^3/kg)$
δ	distance to bracket inflow conductivity peak, m
ρ	formation fluid density, g/cm^3
σ	fluid conductivity, $\mu S/cm$
σ_o	background or residual borehole fluid conductivity, $\mu S/cm$
$\sigma(\tau)$	fluid conductivity at temperature T, $\mu S/cm$
$\sigma(x,t)$	fluid conductivity at position x and time t, $\mu S/cm$
$\bar{\sigma}_L(t)$	average fluid conductivity in the borehole section from L_o to L at time t, kg/m^3
τ	borehole fluid temperature, °C

Subscripts

i	a particular inflow zone (fracture or confined aquifer)
L	at the depth L in the well
max	a local maximum
o	initial or background conditions
w	well conditions

Acknowledgements

Discussions and cooperation with NAGRA personnel, especially M. Thury, A. Zingg, and P. Zuidema are much appreciated. Assistance in computation and graphing from C. Doughty is acknowledged. We would also like to thank C. Doughty, N. Goldstein, and I. Javandel for reviewing and commenting on the manuscript. This work is jointly supported by the Nationale Genossenschaft für die Lagerung radioaktiver Abfälle, Switzerland, and the Director, Office of Energy Research, Office of Basic Energy Sciences, Engineering and Geosciences Division, and the Director, Office of Civilian Radioactive Waste Management, Repository Technology and Transport Program of the U. S. Department of Energy through Contract No. DE-AC03-76SF00098.

Introduction

In the study of the hydrology of fractured rocks, knowledge of the fracture properties is essential. Surface observations may be useful, but the more relevant observations are those made at the depths of interest. Most such measurements are made through boreholes or underground openings. In the case of boreholes various methods of determining fracture properties have been used. For example, a downhole televiewer can be used to map the fracture traces on the borehole walls and determine their density and orientations. However, it is well known that not all of these traces will correspond to water-conducting fractures. Hence there is a need to (1) determine which of the fractures that intersect the borehole actually conduct water and (2) measure directly the hydraulic properties of each such fracture or group of fractures.

Constant pressure, constant flow or pulse tests have been applied to packed intervals along a well bore. Since many of the fractured rocks of interest are of low permeability, the flow rate from a packed interval can be very low. This has necessitated the development of low-flow measurement tools and the use of long-term measurements involving many packed intervals tested one at a time. Packed-off test intervals are usually larger than individual water-conducting zones, thus leading to an uncertainty in the location of a water-bearing fracture. An alternative method is to measure the inflow along the borehole without the use of packers while the well is flowing at a moderate rate. Borehole flowmeters (e.g., Bean, 1971; Hufschmied, 1983; Omega, 1987) can in principle yield the flow rate from individual inflow zones. Flowmeter logs, however, can be strongly affected by well bore radius variations; hence a caliper log has to be run to calibrate the results. Also, there is a low flow rate limit below which the conventional flowmeter log is no longer useful.

A more recent method using a heat pulse for measuring low velocities in boreholes (Hess, 1986; Paillet et al., 1987) can measure much lower flow velocities than conventional flowmeters,

especially when an inflatable packer is used to direct flow through the heat pulse flowmeter. Such packer methods can also be applied as a "skirt" around a borehole flowmeter, such as a spinner, to eliminate the influence of well bore radius variations. This method has been successfully used in some field applications.

The present paper describes a new method involving the use of a time sequence of electric conductivity logs of borehole fluid without the use of packers. Following a description of the logging procedure and the analysis method used, the analytic considerations are presented to show the functional dependence and expected results for the short and long time limits. Then the numerical code used in the data analysis is introduced. Next, a set of data from a deep borehole at Leuggern, Switzerland, is described and our analysis method applied to evaluate the inflow characteristics. The results are then validated against those of independent hydraulic measurements made with the use of packers and against those of chemical sampling and analysis of fracture fluids. Finally, the range of applicability of this technique is discussed in the context of a well test program.

Fluid Conductivity Logging Procedure

Consider the uncased section of a well bore that intersects a number of flowing fractures. In general, the flowing fractures contain fluids with different chemical compositions and ion content from each other, and hence different electric conductivities. The relationship between ion concentration and fluid electric conductivity is reviewed, for example, by Shedlovsky and Shedlovsky (1971), who give graphs and tables relating these two quantities. Hale and Tsang (1988) made a sample fit for the case of NaCl solution at low concentrations and obtained

$$\sigma = 0.187C - 0.004C^2 \tag{1}$$

where σ is the fluid electric conductivity in S/m and C is concentration of NaCl in kg/m^3. The formula is valid at a temperature of 20°C and for values of C up to $\approx$ 6 kg/m^3 and values of σ up to 1.1 S/m (or 11000 µS/cm). The quadratic term can be dropped if one is interested only in values of C up to $\approx$ 4 kg/m^3 and σ up to 0.7 S/m (or 7000 µS/cm) in which case the error will be

less than 10%. In this case we have a convenient linear relationship between σ and C:

$$\sigma(\mu S/cm) = \alpha C(kg/m^3) \tag{2}$$

where $\alpha = 1870\ (\mu S/cm) \cdot (m^3/kg)$; the units given here were chosen because in applications described later in the paper σ is given in $\mu S/cm$.

Suppose the well bore is first washed out with deionized water by passing a tube to the well bottom. There will be some residual ion content and associated electric conductivity. In the field data shown later in the paper, the residual electric conductivity turns out to be about 60 $\mu S/cm$, corresponding to a residual salinity concentration of 0.03 kg/m^3. Now let us produce from the well bore at a flow rate Q. For three fractures we have a situation shown schematically in Figure 1. Note that the flow rates at different parts of the well bore are different, being equal to the sum of all upstream inflow rates. At each fracture inflow point, the parameters characterizing the flow are t_i, the time when the fracture fluid emerges at the well bore; x_i, the location of the inflow point; q_i, the volumetric inflow rate; and $q_i C_i$, the solute mass inflow rate, where C_i is the concentration of ionic solutes in the fracture fluid. Here we have assumed that generally t_i can be different for different fracture inflow points. This could be due to differences in initial values of hydraulic head in these fractures or the specific borehole development and pressure history, with the result that the deionized water enters the fractures during borehole washout. Thus when the well bore is produced at flow rate Q, the deionized water from the fractures first returns to the borehole, delaying the arrival of in situ fracture water.

Figures 2-5 display schematically the salinity distribution inferred from the fluid electric conductivity distribution in the well bore for a series of times. Figure 2 shows the curves for early values of time. In this paper we assume that the well bore cross section is small compared with its length, so that salinity or chemical concentration is uniform at each cross section. If there is no overall upward flow in the well bore and density effects can be neglected, one expects the salinity curves at each inflow point to be symmetrical about the inflow point. When the well is pumped at a given flow rate, a skewing of the curves is expected due to the upward flow in the well bore, which is larger near the well top than near the well bottom.

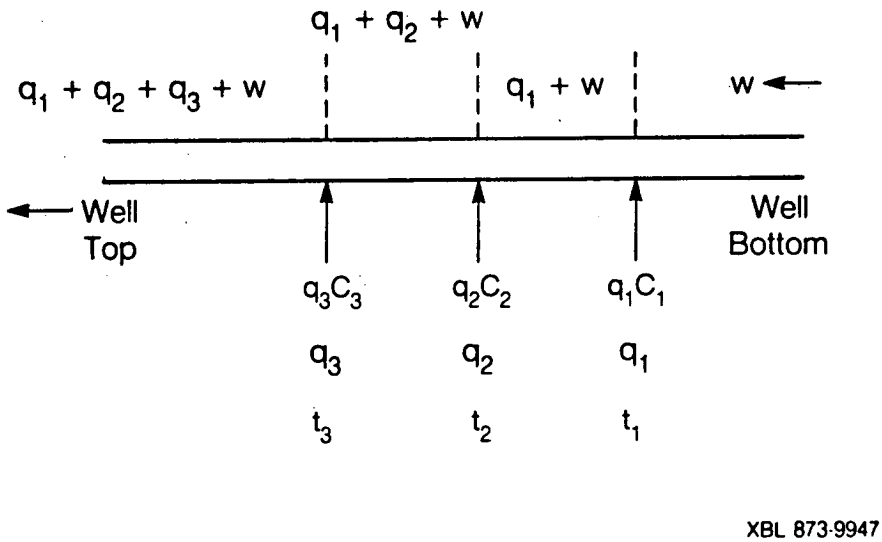

Figure 1. Schematic picture of a well bore with three inflow points and a well bore flow rate w from below.

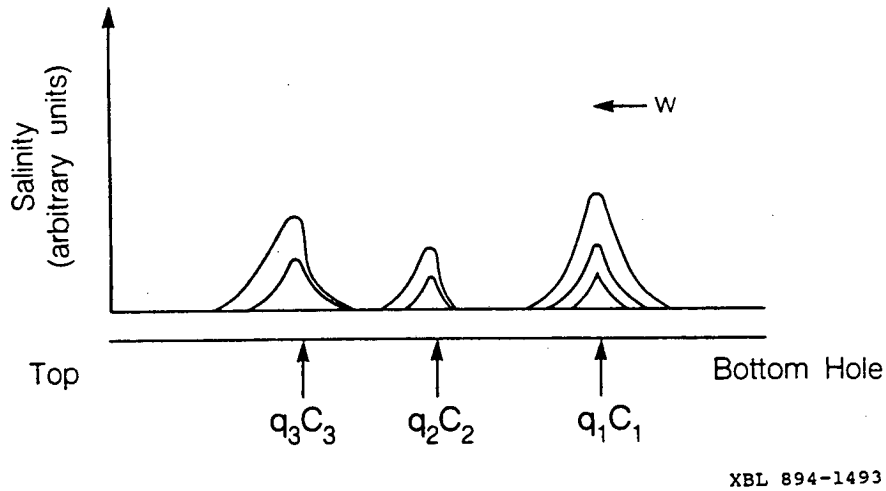

Figure 2. Schematic picture of salinity curves from three inflow points in a well bore at three early times. Higher curves correspond to later times.

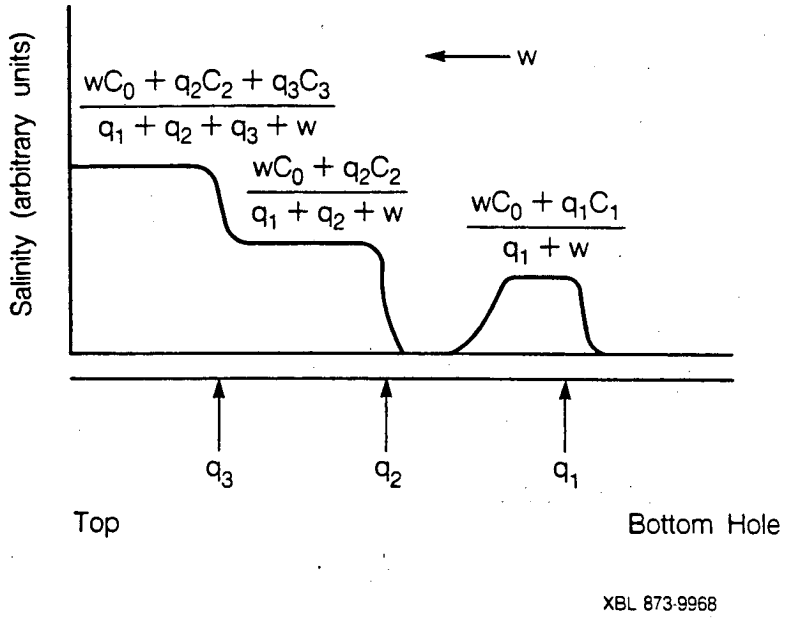

Figure 3. Schematic picture of salinity curves at a large time, assuming very small diffusion effects.

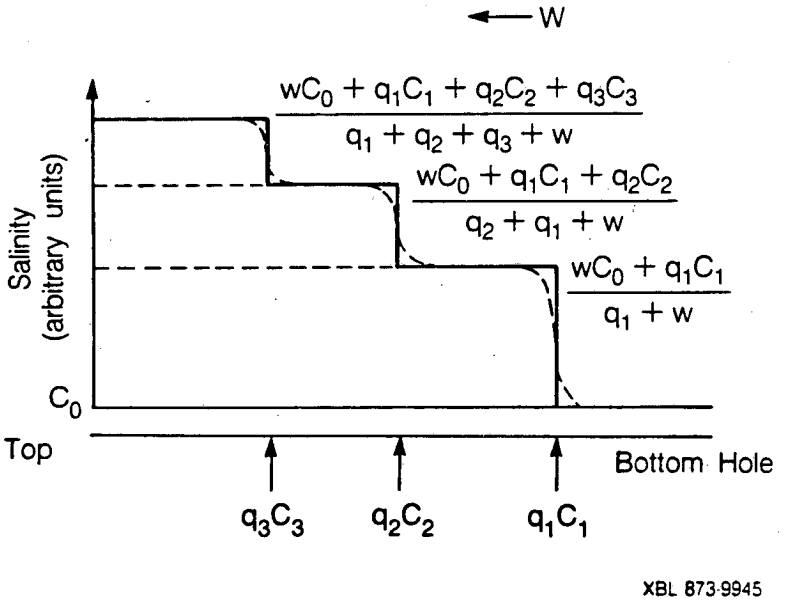

Figure 4. Schematic picture of salinity concentration curves at the very large time limit, assuming very small diffusion effects.

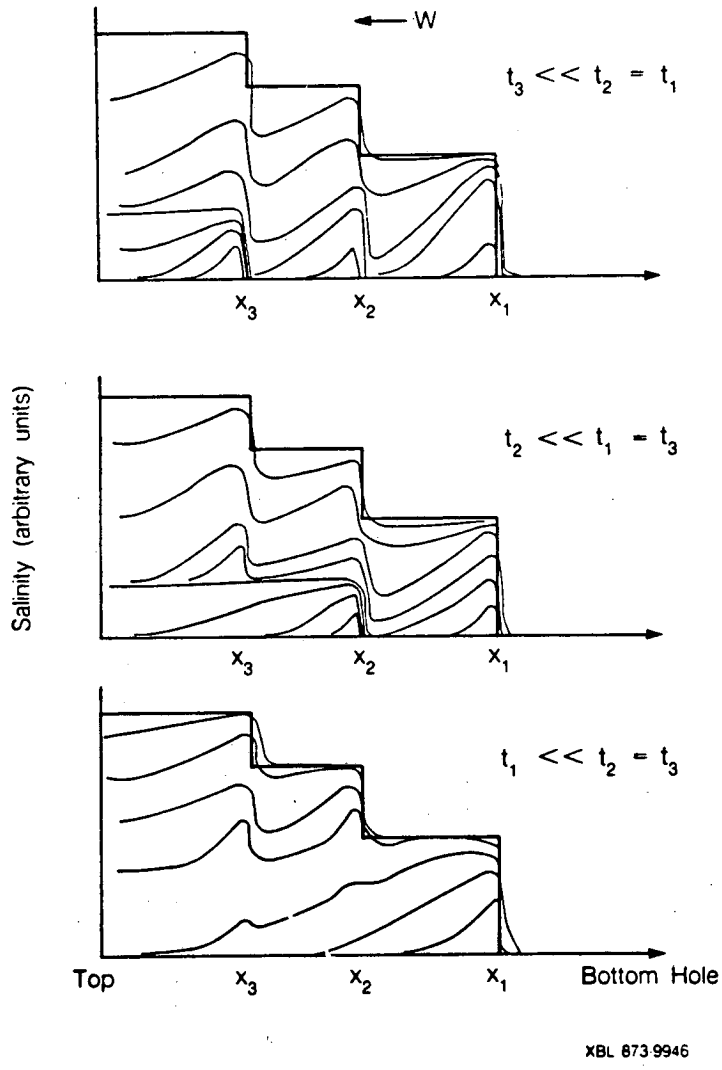

Figure 5. Schematic picture of salinity concentration curves from early to later times, assuming one of the three inflow points begins much earlier than the other two. Lower curves correspond to earlier times.

Figures 3-5 show three possible sets of salinity curves for long time periods, all assuming very small borehole diffusivity. Figure 3 shows one possible set of results. At long times, the saturation salinity is given by

$$C_{max,i} = \frac{wC_o + q_i C_i}{w + \sum_{n=1}^{i} q_n} \tag{3}$$

where q_i is the inflow rate, with i = 1 corresponding to the deepest inflow point of the flow survey (i.e., farthest upstream), w is the borehole flow rate from below the surveyed section, and C_o is the initial salinity of well bore water. If the salinity curves from two inflow points i and i + 1 overlap, then $C_{max,i}$ is still given by (3), but $C_{max,i+1}$ is given by

$$C_{max,i+1} = \frac{wC_o + q_i C_i + q_{i+1} C_{i+1}}{w + \sum_{n=1}^{i+1} q_n} \tag{4}$$

There is a step-jump at the location of each (i+1)-th inflow point when the salinity curve from the i-th inflow reaches the (i+1)-th location. This is demonstrated in Figure 3 for three inflow points, with the second and third inflow salinity curves interfering with each other.

At the limit of very long time periods, the expected salinity curves are shown in Figure 4. Here the step structure is prominent, with the C_{max} value between the i-th and (i+1)-th inflow points given by

$$C_{max,i} = \frac{wC_o + \sum_{n=1}^{i} q_n C_n}{w + \sum_{n=1}^{i} q_n} \tag{5}$$

With diffusion, the step structure will be smeared out as indicated by the dashed lines in Figure 4. Note that the results, equations (3), (4), and (5), are independent of variations of well bore radius.

Figure 5 shows a sequence of curves from early to later times, demonstrating the effect of having one of the three inflows starting much earlier than the other two.

Thus the procedure for fluid conductivity logging is as follows. After the well bore fluid is replaced by deionized water, the well is produced at a low flow rate. Then a fluid conductivity

logging probe is run through the well bore and electric conductivity distribution as a function of depth recorded at several times. Care should be taken not to disturb the well bore fluid to induce large-scale disturbances. The time sequence of fluid conductivity logs can then be used to determine the inflow characteristics of the fractures. For the field case described later in the paper, the well is about 1690 m deep, with the section under survey ranging from 770 to 1637 m below the surface. Each logging run took about an hour, and five logs were taken at intervals of about 4 to 20 hours.

Analytic Considerations

In this section we present a simple analytic method to estimate flow rates q_i and salinity C_i of the fracture fluid. The results will be used later as initial guesses for a detailed numerical fit to field data.

Given a borehole electric conductivity profile $\sigma(x,t)$ measured at a given time, t, such as that given in Figure 2, the area under each peak at x_i can be obtained numerically. This can be simply related to $q_i C_i$, where q_i is the flow rate in m^3/s and C_i is the concentration of the inflow fluid in kg/m^3:

$$\int_{x_i-\delta_1}^{x_i+\delta_2} \pi r_w^2 \, (\sigma(x,t) - \sigma_o) dx = \alpha(q_i C_i)\, t \tag{6}$$

where δ_1 and δ_2 are appropriate distances for bracketing the peak and r_w is the mean well bore radius over this interval; α is a coefficient that relates salinity with electric conductivity (equation 2) and t is time since the fracture fluid began flowing into the borehole. This equation assumes that both q_i and C_i are constant with time. Also the integral on the left-hand side should be evaluated only for relatively early times --that is, before the adjacent peaks overlap significantly, as in Figures 3 and 4.

Equation (6) can be applied to a few conductivity profiles, and a plot of $\int \sigma dx$ against t will give as the slope $(\alpha/\pi r_w^2)\, q_i C_i$ and as the intercept the time t_i when the fracture fluid starts to flow into the borehole.

In principle, once t_i and $q_i C_i$ are obtained for each peak, one can apply late-time results, equations (2)-(5), to calculate the flow rate of the particular inflow point. Thus, from careful measurements of early-time and late-time log data, one can obtain all the inflow flow rates in a simple and straightforward way. These results are not sensitive to moderate variations of well bore diffusivity. Note also that although the early-time results depend on well bore radius, the late-time results are independent of it.

If late-time results are not available, as is usually the case in field experiments, we can use the following method to obtain a good first guess of flow rate q_i from each peak. Figure 6 shows a schematic diagram of a well bore with several inflow points, each with a flow rate q_i, concentration C_i, and position x_i. The total flow rate out of the well is Q, the initial salinity is C_0, and the inflow at the bottom of the well is W. Positions are indicated assuming the origin at the surface and increasing with depth. The total flow rate out of the well is Q, the initial salinity in the well is C_o, and the inflow at the bottom of the well is w. Positions indicated in the figure are depths below the surface.

Let L_o be a reference point near the bottom of the well, upstream (down the borehole) from the first fracture inflow point, and let L be a point up the well from L_o. At L_o, the conductivity is assumed constant and equal to the initial conductivity σ_o. The problem then is to obtain the flow rate Q_L at the point L in the well bore in terms of the electric conductivity log at different times. Q_L is the sum of all of the q_i's between L_o and L, plus the inflow, w, from the bottom of the well at L_o. To simplify the discussion without loss of generality, w will be assumed to be zero in the analysis that follows. Note that taking the difference of two values of Q_L, one upstream from an inflow point and one downstream from the inflow, will yield a value for q_i at that inflow.

If we assume all inflows initiate at the same time (t=0), then the mean concentration, $\overline{C}_L$, in the well bore over the section between L_o and L is given by the salinity of the fluid entering the section at the inflow points minus the salinity of the fluid exiting the section at L with flow rate Q_L:

$$((L_o-L)\pi r_w^2)\overline{C}_L(t) = ((L_o-L)\pi r_w^2)C_o + t \sum_{L<x_i<L_o} q_i C_i - Q_L \int_0^t C(L,t)\,dt \qquad (7)$$

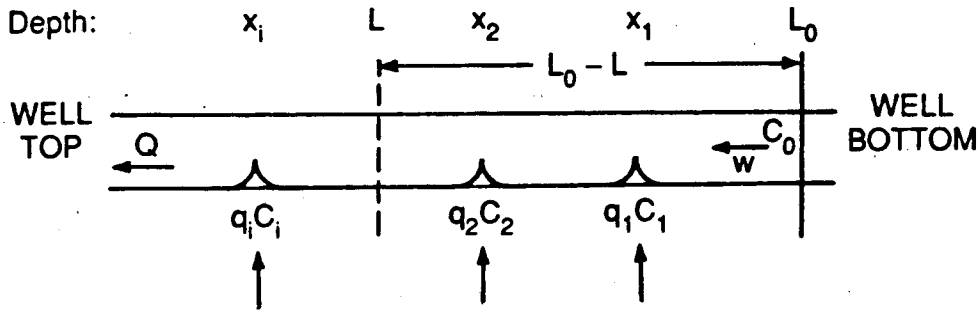

XBL 897-2808

Figure 6. Schematic diagram of a well bore with several inflow points, each with a flow rate Q_i, concentration C_i, and position x_i.

where $(L_o-L)\pi r_w^2$ is the well bore volume in the section between L_o and L, and C(L,t) is the time-varying salinity at the location L. The first term on the right-hand side represents the background mean salinity in the well bore.

If the electric conductivity σ is linearly related to salinity, as in equation (2), we can arrive at the following result by simple algebraic manipulations:

$$Q_L = \frac{\alpha t \sum_{L<x_i<L_o} q_i C_i - ((L_o-L)\pi r_w^2)[\bar{\sigma}_L(t) - \sigma_o]}{\int_0^t (\sigma(L,t)-\sigma_o)\,dt} \tag{8}$$

where $\bar{\sigma}_L(t)=\alpha\bar{C}_L(t)$ and $\sigma(L,t)=\alpha C(L,t)$. Within the uncertainties caused by the approximations previously made, this equation gives the flow rate Q_L at any location L in the borehole directly without requiring a trial-and-error procedure and is valid for any time t.

The first term in the numerator of equation (8) is given by equation (6), which can be applied to profiles at two successive times, t_1 and t_2, near each of these inflow points. We obtain

$$\alpha q_i C_i = \frac{\int_{x_i-\delta_1}^{x_i+\delta_2} \pi r_w^2 (\sigma(x,t_2)-\sigma(x,t_1))\,dx}{t_2 - t_1} \quad . \tag{9}$$

All the quantities in the right-hand side of equation (8) can be obtained from the measured electric conductivity profile.

Note that $(L_o-L)\pi r_w^2$ is an integral quantity representing the total borehole volume over the section $(L_o - L)$. Thus equation (8) is not sensitive to local borehole radius variation, a major advantage over some of the conventional methods of measuring flow rates. Because of the integral forms of the terms in equations (8) and (9), the effects of solute dispersion around the peaks within the interval L_o to L do not affect the results. However, dispersion effects at or near L introduce an error in the value of C(L,t) or σ(L,t). This, we believe, is a major source of uncertainty in our parameter estimation. Examining the values of Q_L determined from equation (8) at a series of locations between two successive peaks illustrates this uncertainty. At these locations, we know that Q_L should be constant. The variation in Q_L is a measure of solute dispersion

in the borehole and can probably be studied to cancel its effect and obtain the proper values of the flow rate. An alternative is to solve for Q_L using equation (8) and then slightly adjust the value to match the field data by using a numerical fitting procedure, which is the approach used in this paper.

If $q_i C_i$ is constant for all inflow points, equation (8) holds for any time t. Thus solving the problem for a few different time periods should give the same result, which is a good internal check. This also means that short-term data may be sufficient to give accurate results. A reduction of the necessary measurement time (say, from 600 hours to 100 hours) represents a major saving in testing cost and makes the technology more commercially applicable.

On the other hand, if any $q_i C_i$ changes with time, Q_L will also change with time. Thus applying equation (8) at different times will tell us (probably crudely) how q_i changes with time. Note that if C_i changes with time, but not q_i, we expect that values of Q_L obtained by equation (8) will be the same for different times (so long as t_2 is set equal to t and t_1 equal to zero in equation (9)). This means that the equation is applicable even when C_i from each inflow point varies with time!

In field operations, because of the fluid logging procedure or changing flow rates (transient effects), it is conceivable that flows from the fractures into the well bore do not initiate at the same time, but at t_i; then an estimate for t_i is obtained as follows:

$$t_i = t_1 - \frac{\int_{x_i-\delta_1}^{x_i+\delta_2} \pi r_w^2 (\sigma(x,t_1)-\sigma_o)\,dx}{\alpha q_i C_i} \tag{10}$$

Equation (8) can also be easily modified to take this intc account:

$$Q_L = \frac{\alpha \sum_{L<x_i<L_o} (t-t_i) q_i C_i H(t-t_i) - ((L_o-L)\pi r_w^2)[\bar{\sigma}_L(t)-\sigma_o]}{\int_0^t (\sigma(L,t)-\sigma_o)\,dt} \tag{11}$$

where $H(t-t_i)$ is the Heaviside step function, which is 1 for $t>t_i$ and 0 for $t\le t_i$.

Here $(t-t_i)q_iC_i$ represents the total salinity input into the borehole from the fracture at x_i during the time $(t-t_i)$. If the conductivity log is measured at time t after the borehole is first washed out with deionized water, we can set $t_1 = 0$ and $t_2 = t$ in equation (9); the total salinity input into the borehole is then given by

$$\frac{1}{\alpha}\int_{x_i-\delta_1}^{x_i+\delta_2} \pi r_w^2\,(\sigma(x,t)-\sigma_o)\,dx \tag{12}$$

regardless of the values of t_i and also regardless whether q_i or C_i is time dependent. Equation (11) can now be generalized to

$$Q_L = \frac{\sum\limits_{L<x_i<L_o}\int_{x_i-\delta_1}^{x_i+\delta_2} \pi r_w^2\,(\sigma(x,t)-\sigma_o)\,dx \;-\; ((L_o-L)\pi r_w^2)[\bar{\sigma}_L(t)-\sigma_o]}{\int_0^t (\sigma(L,t)-\sigma_o)\,dt} \tag{13}$$

Here Q_L has to be interpreted as a type of mean flow rate over the time period 0 to t at location L. So far we have only applied equations (6) to (10) to a field case presented below. We have plans to study the use of equations (12) and (13) for time-varying q_i and C_i.

Equation (8) assumes that all solute is flowing up the well bore and thus does not apply to locations in the well bore where the solute flux is mainly down the borehole by diffusion. This is not a major restriction because avoiding these locations does not prevent us from obtaining the flow profile in the well bore. In principle, all we need is to apply the equation to a point at the downstream side (up the borehole) of each inflow point.

A special case is when $(L_o - L)$ is small and L is below (or upstream of) the first inflow point. If we apply equation (8) in this case, we obtain the indeterminate result Q_L=0/0. This is not surprising, indicating the simple result that without input salinity in the section of interest, it is not possible to determine the flow rate.

The formulas in this section have been programmed into a simple code, called PRE.

Numerical Method

For a general problem of multiple inflow points, overlapping salinity curves and variable dispersion coefficient K, no analytic solution is readily available and numerical methods are required. For our purpose, we developed a simple computer code (Hale and Tsang, 1988) that solves the linear advective-dispersive equation

$$K \frac{\partial^2 C}{\partial x^2} - v \frac{\partial C}{\partial x} + G = \frac{\partial C}{\partial t} \tag{14}$$

where C is the concentration of solute, K is the dispersion coefficient, v is the linear borehole fluid velocity, and G is the source term corresponding to q_i and C_i at various fracture inflow locations. The dispersion coefficient K can be set constant or proportional linearly or quadratically to velocity. The initial condition is

$$C(x,0) = \frac{\sigma_o}{\alpha} \tag{15}$$

over the region of interest in the borehole. The code uses a finite-difference solution scheme with upstream weighting and can accommodate various boundary conditions. It has been verified against a number of analytic solutions and also against a well-validated numerical code, PT (Bodvarsson, 1982; Tsang 1985; Tsang and Doughty, 1985). For easy reference later, we have called this code BORE.

Let us now present a few results of fluid salinity behavior in the well bore using BORE with constant K to confirm the earlier schematic and analytic considerations and to study parameter sensitivities. Figure 7 shows the numerical results of a case with one inflow point under an overall inflow rate w. Figure 8 shows a late-time numerical solution for the case of the overall well bore fluid flow rate w equal to 0, q/3, or q, where q is the fracture inflow rate. The saturation salinity values are C, ¾C, and ½C, respectively. It should be noted that Figures 7-10 assume that the salinity of the upstream fluid is zero. This is obvious from the proportionate mixing of inflow salinity with the upcoming well bore flow with $C_o = 0$ (equation 3). Note that we are using the volume flow rates w and q and not linear velocities. Thus the variation of well bore cross section has no effect on these results.

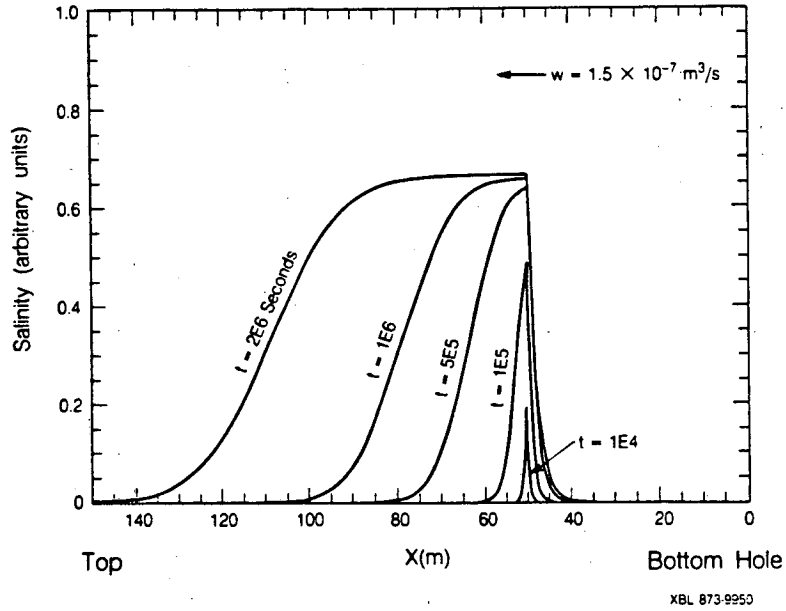

Figure 7. Numerical results for one inflow point from early to late times.

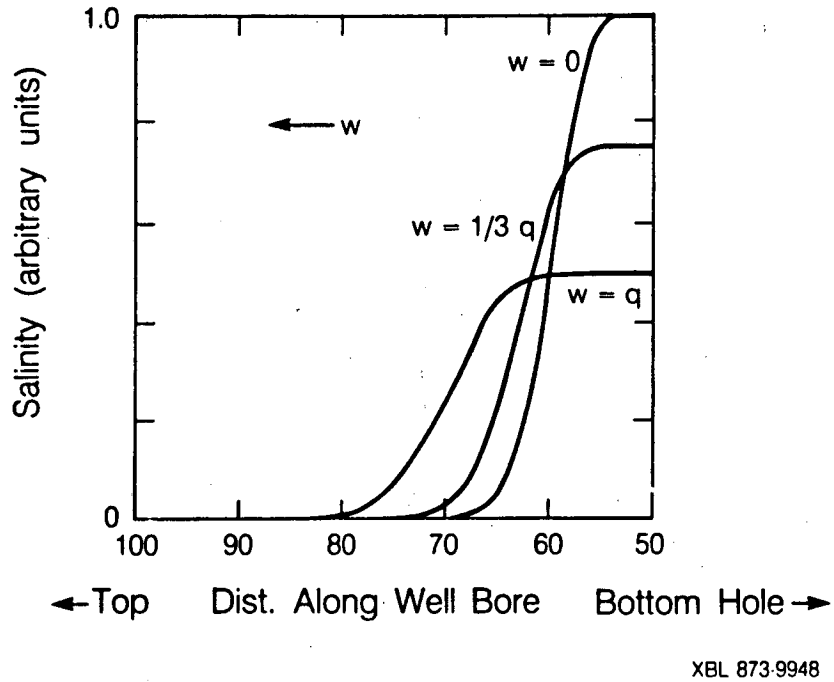

Figure 8. Numerical results for one inflow point at flow rate q for three values of well bore flow rate from below: w = 0, w = q/3 and w = q.

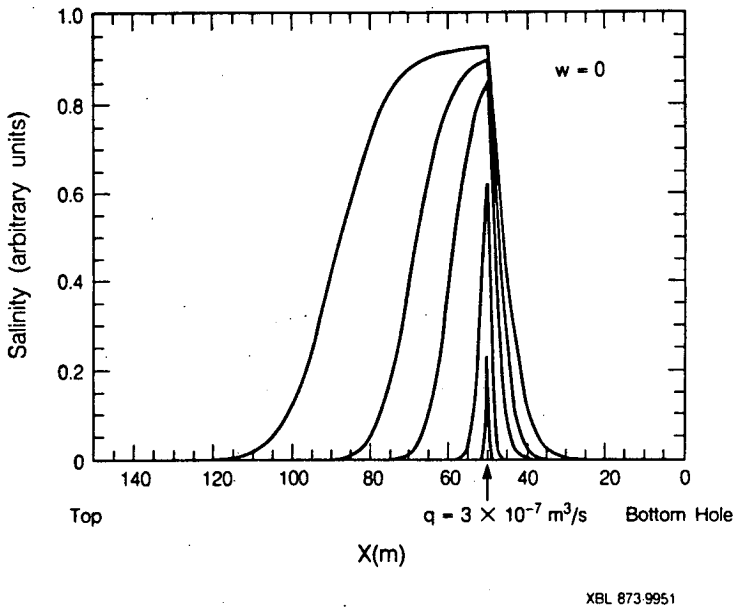

Figure 9. Numerical results for one inflow point and w = 0 for dispersion constant K equal to 50 m^2/s.

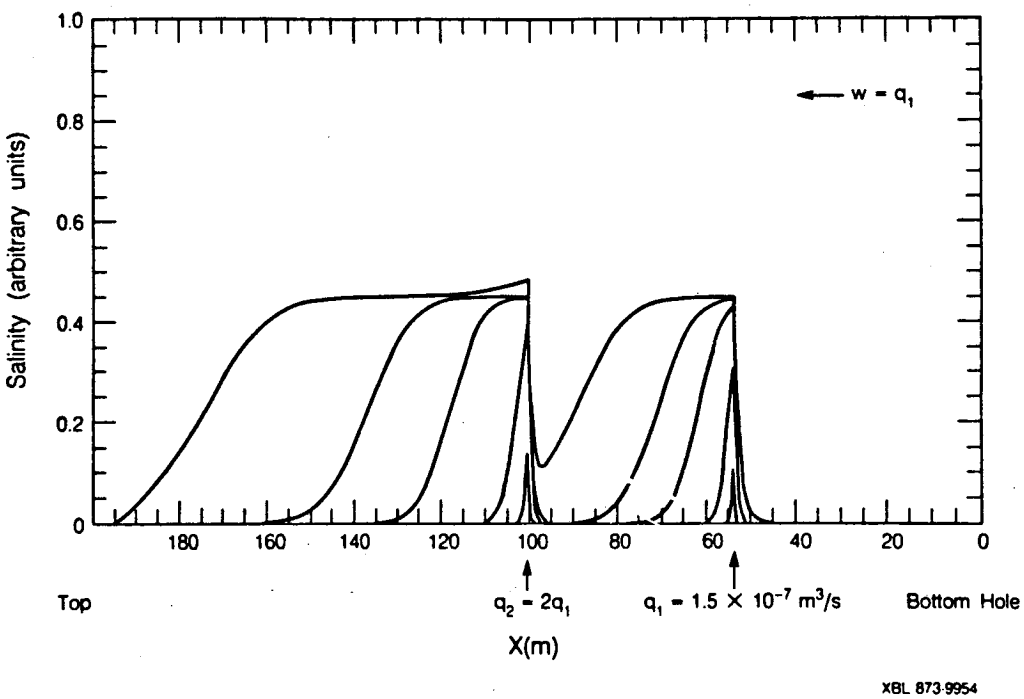

Figure 10. Numerical results for two inflow points.

Figure 9 shows the salinity curves in the well bore w = 0. Because there is a closed boundary at well bottom x = 0, there is still a preferred flow upwards. This can be seen easily if the closed boundary is represented by image sources below it. With inflow at rate q at the point x = 50 m, the flow rate in the well bore is q downstream from x = 50 m and 0 upstream.

Figure 10 shows the interference between two inflow points. We have taken the K value to be 1.25×10^{-5} m^2/s and the overall well bore flow rate to be $w = 1.5 \times 10^{-7}$ m^3/s. The two inflow points are at x = 50 m and x = 100 m with flow rates $q_1 = 1.5 \times 10^{-7}$ m^3/s and $q_2 = 3 \times 10^{-7}$ m^3/s. Interference effects are seen as a sudden jump in the curve when the salinity curve for the upstream inflow point overlaps that for the downstream point. Figure 10 also shows the large time period results with a step structure at large times confirming that shown in Figure 4.

Application to a Synthetic Data Set

A synthetic data set composed of a time-series of conductivity logs with times ranging from 0.5 to 600 hours was generated by the code BORE. Four inflow points were used. The synthetic logs for 0.5, 144, and 600 hours are shown in Figure 11. The data set is designed to be realistic, similar to a real field case described in the next section.

PRE was then used to estimate the inflow parameters using various subsets of the time-series of logs, with successively larger final times (i.e., using the first five logs, the first eight, the first ten, etc.). The resulting estimates of the parameters, shown in Table 1, indicate that the values stabilize at relatively short times (less than 100 hours) and that the use of additional logs provides little additional information. This may mean that the test need be carried out for only 100 hours. The reason is is that the values of $q_i C_i$ are based on early times, and the data at later times only enter into the integral in the denominator of the equation for Q_L.

The predicted profile of conductivity logs based on parameters obtained by applying PRE to the 96-hour data is shown in Figure 12. The agreement with the synthetic data is already very good, with the exception of the inflow at 915 m. Minor adjustments result in a good fit to the synthetic data, as shown in Figure 13.

Table 1. Parameter Estimates for Synthetic Case

Time of Latest Log (hrs)	Inflow Rate (L/min)			
	q_{850}	q_{915}	q_{1200}	q_{1440}
8	5.5	0.26	0.20	0.14
12	5.2	0.26	0.20	0.14
24	5.0	0.27	0.20	0.12
48	5.0	0.27	0.20	0.11
96	4.9	0.27	0.21	0.095
144	4.9	0.28	0.21	0.089
288	4.9	0.28	0.22	0.082
600	4.8	0.28	0.22	0.078
Fit by adjustments from 96	4.8	0.23	0.24	0.066
Input	4.3	0.27	0.22	0.070

Time of Latest Log (hrs)	Inflow Concentration (kg/m^3)			
	C_{850}	C_{915}	C_{1200}	C_{1440}
8	0.74	3.1	0.75	0.36
12	0.77	3.2	0.76	0.36
24	0.81	3.1	0.76	0.41
48	0.81	3.1	0.74	0.47
96	0.82	3.0	0.72	0.54
144	0.83	3.0	0.70	0.58
288	0.83	3.0	0.69	0.63
600	0.83	3.0	0.68	0.66
Fit by adjustments from 96	0.85	3.1	0.68	0.72
Input	0.85	3.1	0.68	0.71

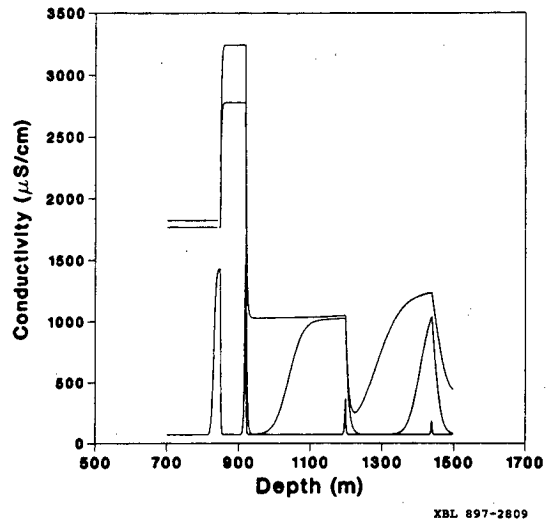

Figure 11. Synthetic results at 0.5, 144 and 600 hours (from lower curve to highest curve respectively).

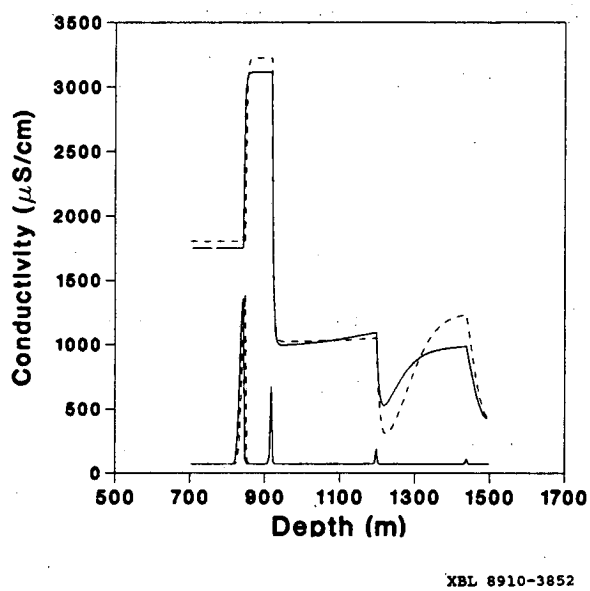

Figure 12. Results of synthetic initial estimate for two times, 0.5 and 600 hours, using 96-hour data.

In order to understand the effects of adjusting the various parameters, a sensitivity study was conducted. An initial set of parameters, the "base" case, is shown in Table 2; this is a slight variation on the case shown in Table 1. The effects of changes in K, q_i, C_i, and $q_i C_i$ are shown in Figures 14, 15, 16, and 17. All of these figures depict the concentration profile at 48 hours, with the dashed line showing the profile for the base case, and the solid line showing the effect of parameter modification.

Figure 14 shows the effect of decreasing K by a factor of 100. Aside from the deepest inflow, where diffusion is a significant transport mechanism, the effects of a change of two orders of magnitude are small. Figure 15 shows the effect of increasing q_i by a factor of 2 and decreasing C_i accordingly in order to keep the same mass inflow value. The effect is substantial and increases as the total flow rate increases up the borehole. Figure 16 shows that the mass inflow is decreased by a factor of 2, as is the concentration; the flow rate is kept the same as in the base case. Decreasing the inflow concentration obviously decreases the concentration profile in the borehole, but the general shape is the same as the base case. This is in contrast with Figure 17 where the flow rate is decreased and the concentration kept the same, again using a factor of 2. The smaller flow rate has significant effects on the conductivity profile. These parameter variation studies provide guidance to numerical fitting of data using BORE.

Field Experiment and Data Analysis

The borehole at Leuggern is one of six boreholes studied by Nationale Genossenschaft fur die Lagerung radioaktiver Abfalle (NAGRA) as part of a regional investigation program in northern Switzerland. As shown in Figure 18, the borehole is located near the confluence of the Rhine and Aare Rivers in the Table Jura south of the Black Forest Massif. Drilling of the borehole began in June 1984 and was completed in February 1985 at a total apparent depth along the borehole of 1688.9 m. The borehole deviates slightly from vertical, and thus the true terminal depth of the borehole below the ground surface is 1631.6 m. In this paper, depth is measured along the borehole.

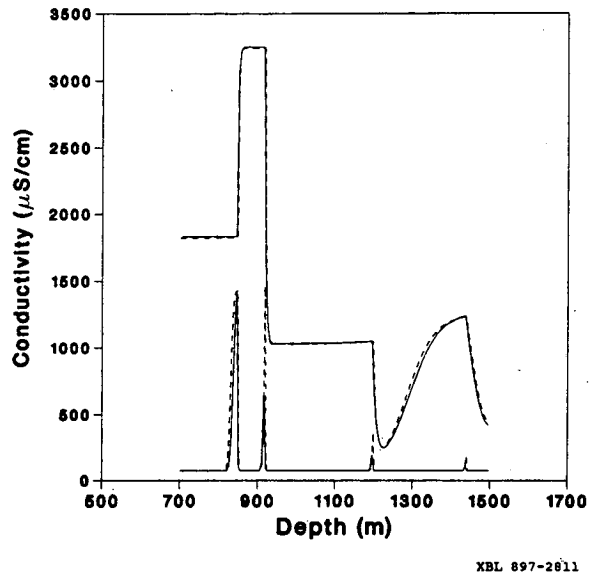

Figure 13. Results after adjusting parameters for the synthetic case. Results for 0.5 and 600 hours are shown.

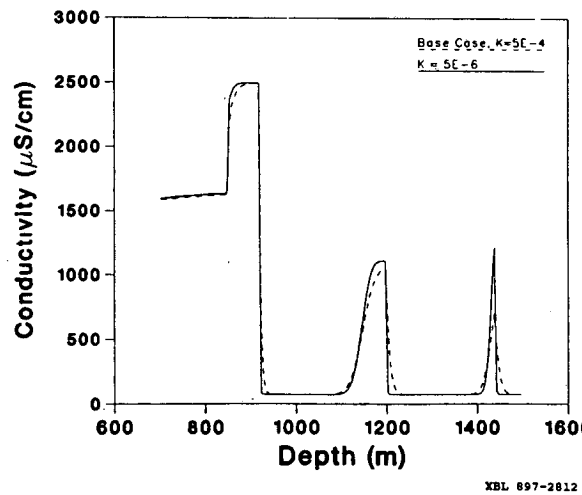

Figure 14. Sensitivity to K variation.

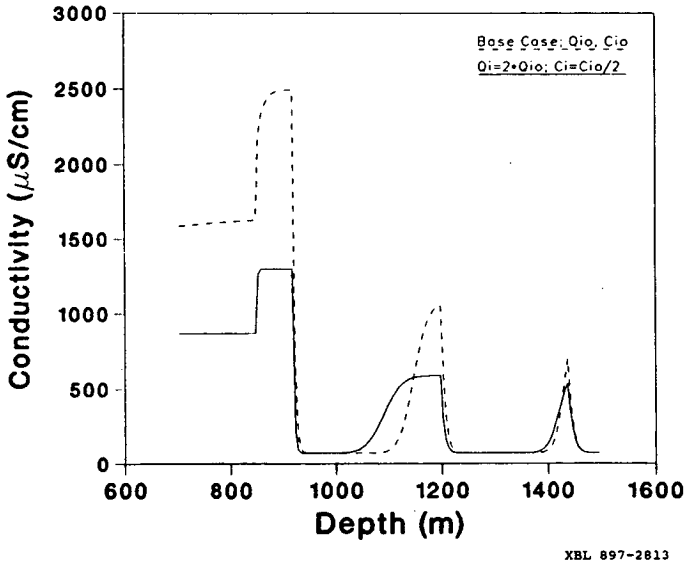

Figure 15. Effect of increasing q while maintaining constant qC.

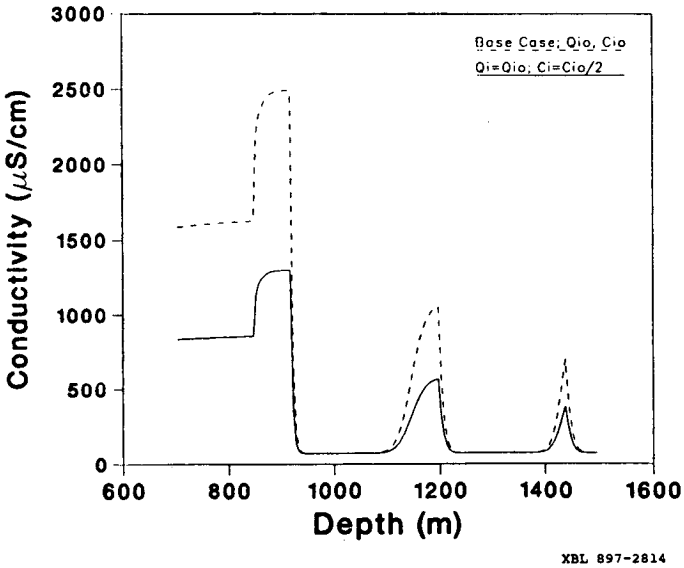

Figure 16. Effect of decreasing C and qC.

Table 2. Parameters used in sensitivity analysis: Base case

x_i (meters)	t_i (hours)	q_iC_i (10^{-6}kg/s)	q_i ($10^{-6}m^3/s$)	C_i (kg/m^3)
1440	0	0.7	1	0.7
1200	0	2.8	4	0.7
918	0	12	4	3.0
843	0	56	70	0.8

$K = 5.0 \times 10^{-4} m^2/s$
$Q = 7.9 \times 10^{-5} m^3/s$

The geology intersected by the borehole is described in Figure 19. A thin layer of unconsolidated Quaternary deposits is underlain by consolidated Triassic sediments consisting of the Muschelkalk and Buntsandstein. The base of the Buntsandstein group lies unconformably on crystalline rock consisting of biotite-gneiss to a depth of 1387.3 m and biotite-granite from 1387.3 m to 1688.9 m. The Leuggern borehole contains casings of various diameter at various depths. Of interest here is the final casing, of 0.17 m diameter, which was cemented at a depth of 557.5 m in the crystalline rock. Nominal borehole diameter below the casing is 0.14 m down to the final depth.

A suite of investigations was conducted in the borehole, including core logs, geophysical logs, hydraulic packer testing, and hydrochemical sampling. A brief overview of the standard testing program in the NAGRA deep boreholes in northern Switzerland and the results are provided by Thury and Gautschi (1986).

Fluid logging experiments were carried out by NAGRA in different boreholes during 1985. Measurements from the Leuggern borehole are taken as an example to demonstrate the applicability of the method. A production-injection packer (PIP) was set at 1637 m to shut off a highly permeable section near the bottom of the borehole and isolate it from the low-permeability section between 770 m and 1637 m, which was studied by the fluid log measurements. First the borehole water was replaced by deionized water through a downhole tubing, and the fluid conductivity was measured at the outflow at welltop to stabilize at 60 µS/cm. Then the tubing was

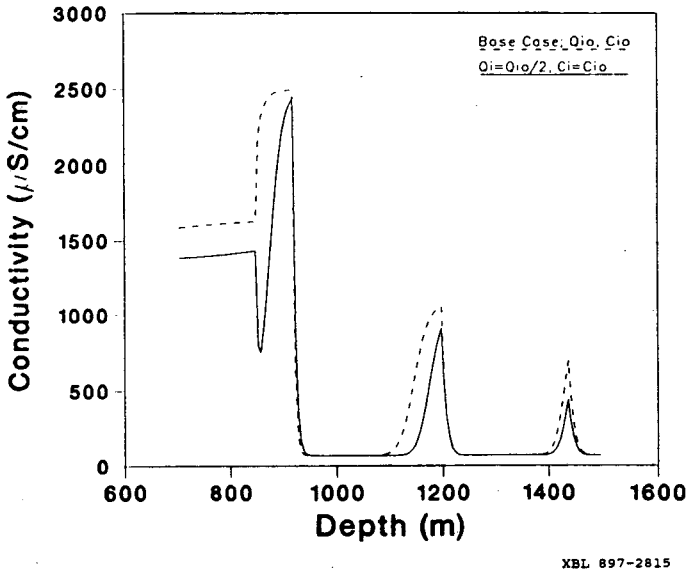

Figure 17. Effect of decreasing q and qC.

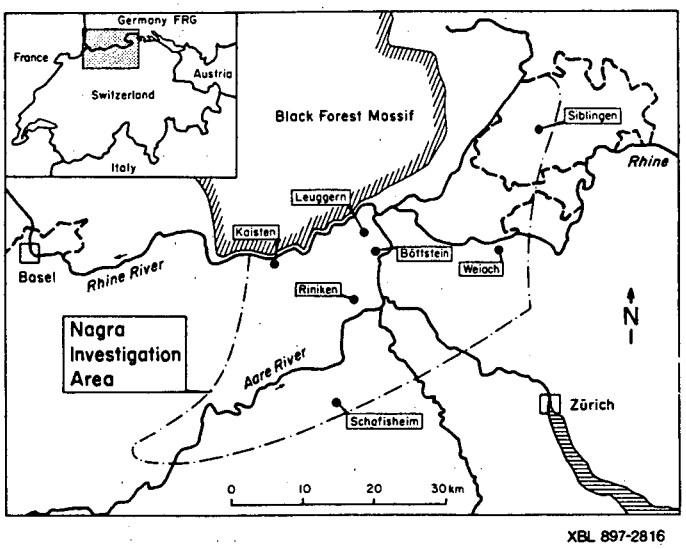

Figure 18. Map of Northern Switzerland, with the location of the Leuggern borehole.

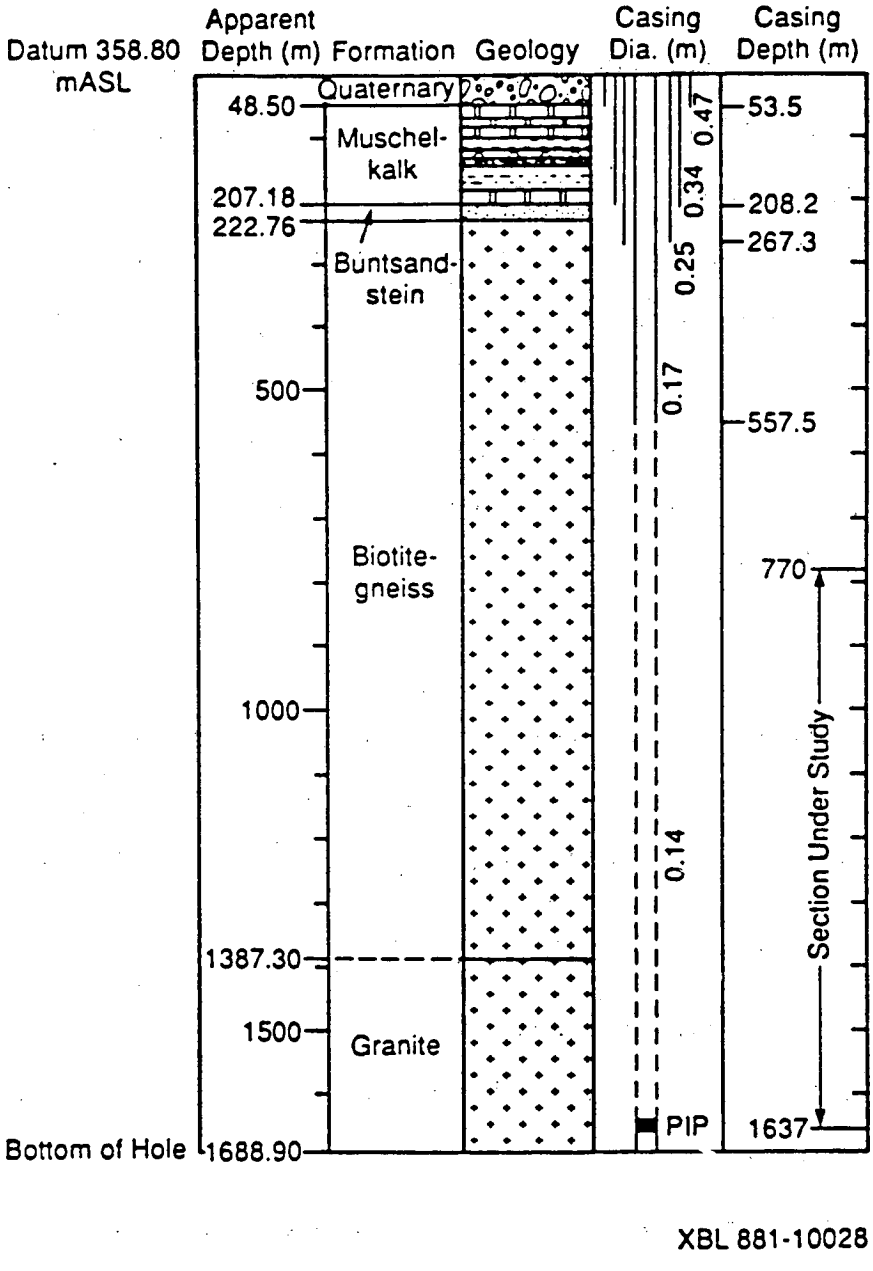

Figure 19. Geological formation intersected by the Leuggern borehole, and other borehole characteristics.

pulled out of the well and a pump placed at a depth of 210 m, and background temperature and electric conductivity logs were taken. Then with pumping maintained at about 20 L/min a series of five complete electric conductivity logs were taken over 2 days. After that a temperature log was again taken.

The conductivity logs are shown in Figures 20 and 21. Figure 20 shows only the upper portion of the section studied (700-1000 m), displaying two inflow points; Figure 21 shows the full section, displaying nine major inflow points. For the sake of identification, these peaks are labeled 1 through 9 in the figures. The well bore diameter over the section is 5.5 inches, or 14 cm. In these figures, the sharp peaks at early times are characteristic of fracture inflows. If the inflows were from a porous medium layer, the peaks would be flat-topped for all times. The association of these peaks with fractures intercepted by the well bore has been confirmed by televiewer logs. The temperature log shows an increase of temperature with depth that can be approximated adequately by

$$\tau = 10 + \frac{x}{30} \tag{16}$$

where x is in meters and τ in °C. The fluid electric conductivity, σ, depends on temperature. In order to convert the measured values shown in Figures 20 and 21 to normalized conductivity values at a uniform temperature, of 20°C, the following formula (NAGRA, 1987) is used:

$$\sigma\,(20°C) = \frac{\sigma(\tau)}{1 + 0.022\,(\tau - 20)} \tag{17}$$

The field data are digitized and then normalized according to equations (16) and (17). The normalized electric conductivity log is shown in Figure 22. Now we proceed to study and match the nine peaks in this figure.

The positions of the nine peaks range from the deepest (peak 1) at x = 1440 m to the shallowest (peak 9) at x = 843 m. We have selected an arbitrary starting time of pumping as a reference. Peaks 8 and 9 have data at 13.03 hours relative to this reference time. All peaks have data at 27.12, 31.28, 38.41, and 57.24 hours. We consider the starting times of these inflows to be unknown and possibly different from each other. First let us treat these peaks independently and

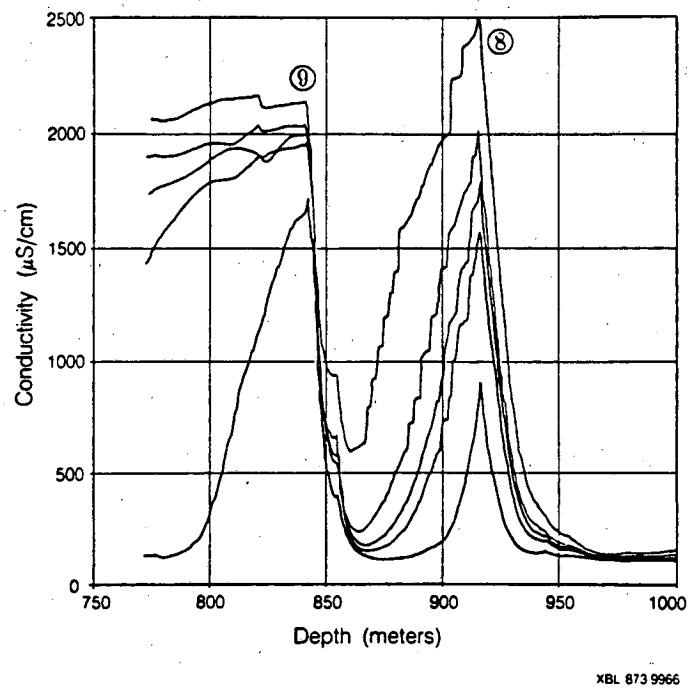

Figure 20. Field fluid-conductivity log data from NAGRA (1986) for the 770-1000 m section of a 1690-m borehole.

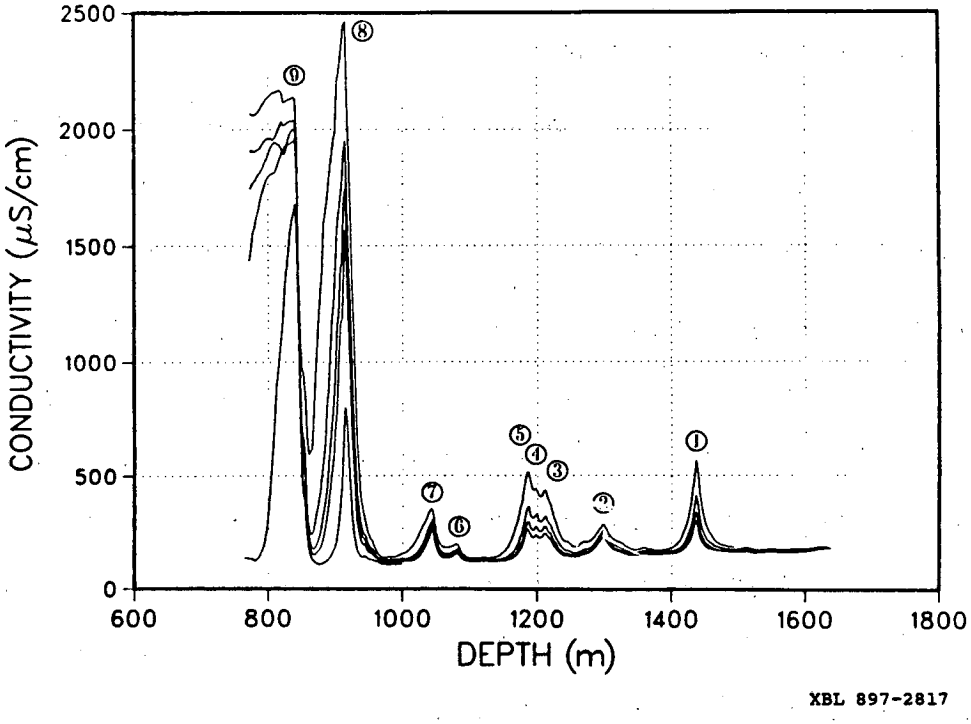

Figure 21. Field fluid-conductivity log data from NAGRA (1986) for the full logged 770-1610 m section of a 1690-m borehole.

apply the results from equation (6), after we convert the concentration C to conductivity values σ by means of equation (2). Figure 23 shows the plot of $\int \sigma(x,t)dx$ versus time t. The slopes and intercepts of the early times are listed in Table 3.

The set of four logs, which cover the entire section, were used as input to PRE. The initial estimate of the inflow parameters is shown in Table 4. The values for t_i, q_iC_i, and q_i were obtained using equations (10), (9), and (13), respectively. C_i was obtained by dividing q_iC_i by q_i. Inflows 4 and 5 were combined, as well as inflows 6 and 7, because of the small mass inflows found at 4 and 6. The total flow rate was estimated at 3.9 L/min.

These parameters were used as input to BORE for detailed adjustment numerically to get the fracture inflow parameters, and the results before parameter adjustments are shown in Figure 24. It is obvious from that the flow rate for the inflow from 4 and 5 has been overestimated, and all concentrations downstream from that point are diluted. The first steps in adjusting the parameters would be (1) to force the separation of inflows 4 and 5 and 6 and 7 by dividing the mass inflow between them and (2) to scale down the flow rate at inflow 4/5 and increase the concentration in order to preserve the initial qC estimate.

After adjusting the estimated inflow parameters obtained from PRE, examining the results from BORE, and repeating the cycle of adjustment and comparison of profiles, a final fit was obtained, as shown in Table 5. Figure 25 shows the results of this fit at various times.

A number of features of Table 5 may be pointed out here. First, total flow rate Q is estimated to be 2.1×10^{-5} m^3/s, which is an order of magnitude smaller than the pumping rate at the top of the well, 20 L/min (or 33×10^{-5} m^3/s). We find that it is impossible for us to arrive at the higher total flow rate by our fitting procedure. A later review of experimental conditions showed that most of the large flow rate may be taken up by inflows between depths of 500-770 m and that the total flow rate from the section 770 to 1637 m may well be much smaller. Second, the estimated flow rates q_i, with values from 0.2 to 17×10^{-6} km^3/s (0.01 to 1 L/min), may represent the range of sensitivity for the fluid conductivity logging method under the particular field arrangement. Third, from Table 5, it is noted that the salinity C_i for peak 8 is a factor of 5

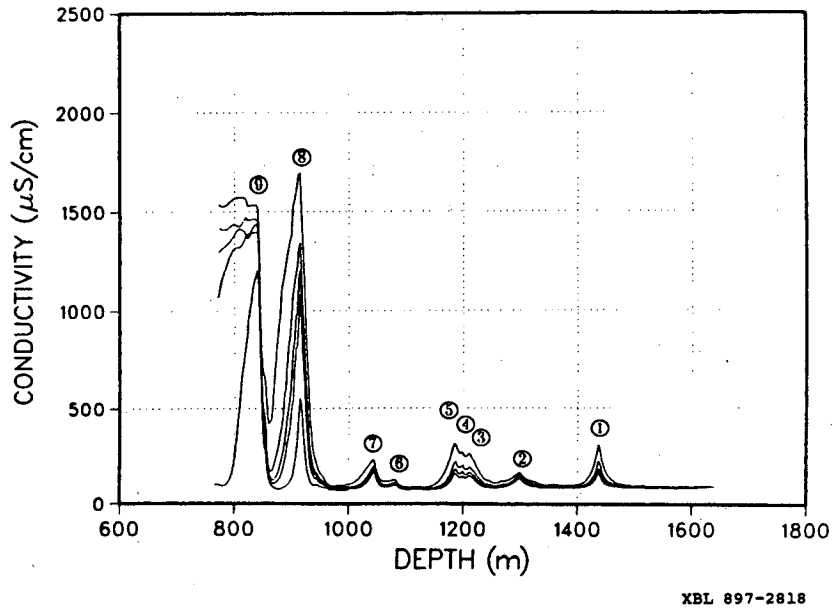

Figure 22. Normalized fluid-conductivity log data.

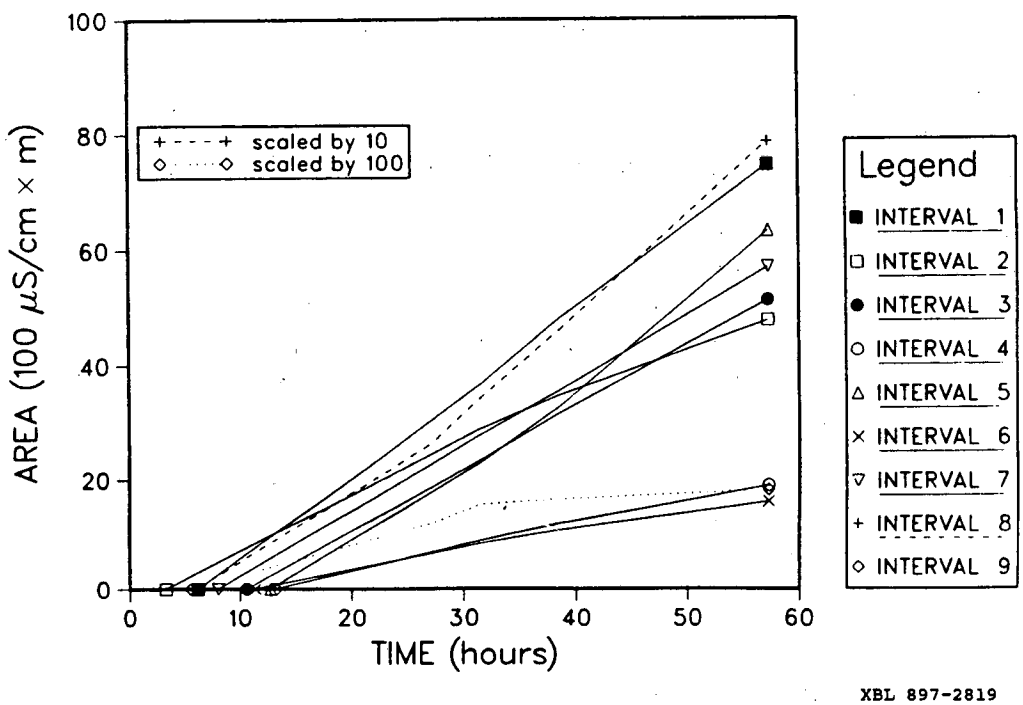

Figure 23. Area versus time plots for all nine inflow points.

Table 3. Data from $\int\sigma(x,t)\,dx$ vs t curves.

Peak No.	x_i (meters)	Intercept (hours)	Slope (100 μS/hr)
1	1440	6	145
2	1300	3	102
3	1215	11	111
4	1200	13	47
5	1188	13	121
6	1085	11	40
7	1048	8	118
8	918	6	1243
9	843	6	(5449)

Table 4. Parameters used in initial match of field data.

Peak No.	x_i (meters)	t_i (hours)	q_iC_i (10^{-6}kg/s)	q_i ($10^{-6}m^3/s$)	C_i (kg/m^3)
1	1440	16	0.33	2.0	0.16
2	1300	15	0.27	4.7	0.057
3	1215	16	0.25	0.36	0.68
4 & 5	1188	27	0.38	37	0.010
6 & 7	1048	24	0.36	0.10	3.5
8	918	13	4.1	3.5	1.2
9	843	11	16	17	0.97

$K = 5.0\times10^{-4} m^2/s$
$Q = 6.5\times10^{-5} m^3/s$

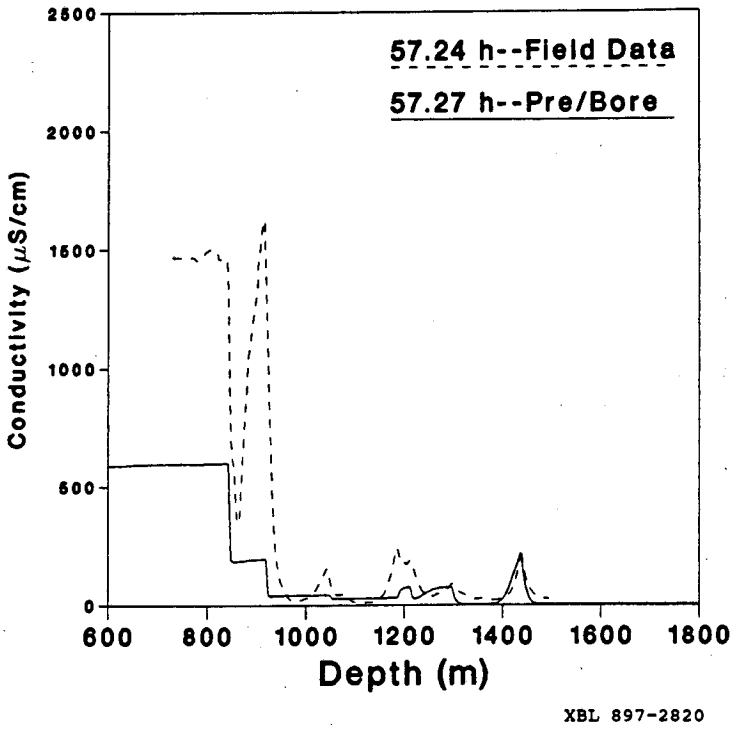

Figure 24. Initial fit to field data.

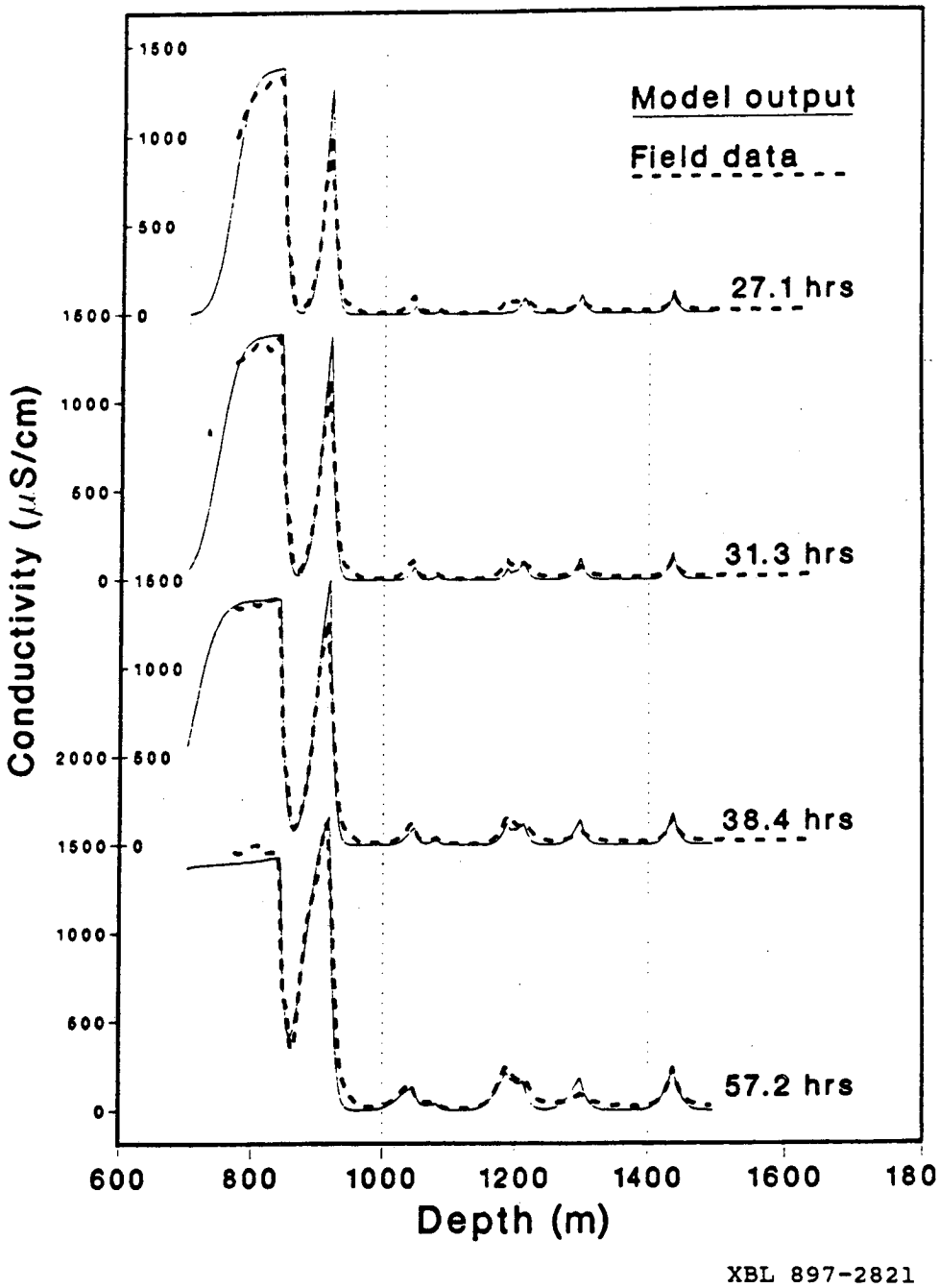

Figure 25. Final fit to field data.

Table 5. Parameters used in final match of field data.

Peak No.	x_i (meters)	t_i (hours)	q_iC_i (10^{-6}kg/s)	q_i (10^{-6} m^3/s)	C_i (kg/m^3)
1	1440	16	0.33	0.65	0.50
2	1300	15	0.27	0.60	0.45
3	1215	16	0.25	0.55	0.45
4	1200	27	0.10	0.25	0.40
5	1188	27	0.28	0.65	0.43
6	1085	24	0.074	0.20	0.37
7	1048	24	0.29	0.60	0.48
8	918	13	4.1	0.75	5.5
9	843	11	16	17	0.95
$K = 1.0 \times 10^{-3}$ m^2/s					
$Q = 2.1 \times 10^{-5}$ m^3/s					

larger than that for peak 9 and an order of magnitude larger than that for the others. These results will be used below for validation against chemical sampling data from the same borehole.

Estimation of Transmissivities from the Results of Fluid Conductivity Logging

The results of fluid conductivity logging, i.e., the inflow rate produced from each fracture intersected by the borehole, can be combined with other observations made during the time of pumping to calculate the transmissivity of each of the fractures or fracture zones. These calculations make use of the basic equation describing the unsteady flow of water to a well in a confined aquifer and its analytical solutions under various assumptions. Essentially, each water-producing fracture is treated as a single confined aquifer that can be readily analyzed using classical well testing techniques.

The general solution of the unsteady flow of water to a well in a confined aquifer has been given by the classical papers of Theis (1935) and Jacob (1940). For the case of a small-radius well or long time values, this solution may be approximated (Cooper and Jacob, 1946) by

$$s(r_w,t) = h_o - h(r_w,t) = \frac{Q_w}{4\pi T} \ln \left[\frac{2.25Tt}{r_w^2 S} \right] \tag{18}$$

where s is the drawdown, h_o is the initial uniform head in the aquifer, Q_w is the discharge from the well, T is the transmissivity of the aquifer, S is its storativity, r_w is the well radius and $h(r_w, t)$ is the transient head in the well opposite the inflow zone. Below we shall also use specific storage S_s which is defined as the product of storativity with the aquifer thickness.

For a well intersecting multiple confined aquifers or fractures, equation (18) is generalized to yield a relationship between drawdown s_i in the well, inflow q_i, transmissivity T_i, storativity S_i, and well radius r_{w_i} as follows:

$$s_i(r_{w_i},t) = h_{o_i} - h_i(r_{w_i},t) = \frac{q_i}{4\pi T_i} \ln \left[\frac{2.25T_i t}{r_{w_i}^2 S_i} \right] \tag{19}$$

where i indicates parameters that may be different for each of the permeable zones or fractures intersected by the borehole.

In order to use equation (19) to determine the transmissivity T_i of each permeable zone, several parameters must be known, they are (i) the drawdown $s_i(r_{w_i},t)$ in the well, (ii) the steady discharge q_i from each zone, (iii) the elapsed time of pumping t, (iv) the well radius r_{w_i}, and (v) the storativity S_i of each zone.

The drawdown s_i opposite each flowing zone is a function of the initial head h_{o_i} in each zone and the head h_i in the well at that zone. If the formation head is uniform, the initial head is simply the steady-state head in the borehole prior to pumping. If the formation head is nonuniform, it can be, in principle, derived from hydraulic testing results such as those presented in Belanger et al. (1988) for the Neuggern borehole. Alternatively, h_o may be estimated by means of fluid logging from a comparison of two flow states, e.g., a first flow state with no pumping from the well and a second flow state with pumping (Huf- schmied, 1983). If there is no flow observed in the well without pumping, the formation head along the borehole can be assumed uniform and in equilibrium with the head in the borehole prior to pumping. On the other hand, flow in the well without pumping would indicate head differences between the various permeable

zones intersected by the borehole.

In the Leuggern borehole, some head measurements were known from single and double packer testing conducted prior to the fluid electric conductivity logging (Belanger et al., 1988). Freshwater heads varied between only 362 m above sea level (a.s.l.) at a depth of 850 m and 356 m a.s.l. at a depth of 1600 m. The closeness of these values to the annulus conditions at the surface elevation of 358.8 m a.s.l., and the relatively low mineralization of the formation and borehole fluids justify the use of a uniform initial head at 359 m a.s.l. for all permeable zones in the test section under study. Slight differences in the initial conditions on the order of a few meters are relatively unimportant compared to the large drawdown of the water table in the borehole at late time amounting to 176 m.

The head h_i in the well opposite each flowing zone during the pumping phase of the fluid conductivity test is primarily a function of the imposed drawdown at the pump. In addition, the salinity and temperature of the borehole fluid are gradually changing with time, which causes the density profile to be time-dependent. Such density effects can easily be accounted for, since electric conductivity and temperature of the borehole fluid is periodically monitored throughout the borehole. Additionally, head corrections for friction and inertia effects could also be incorporated because the volumetric flow rate along the borehole is also known. An appropriate method is described in Hufschmied (1983). However, given the large drawdown of 176 m at the pump, the low salinity of the inflowing formation water, the approximately compensating effects of the increasing temperature on the density and the low flow rate, none of the above corrections was deemed necessary, and thus the observed drawdown at the pump of 176 m at late times is applied to all permeable zones between 770 and 1637 m depth.

The volumetric fluxes q_i from each interval are taken from the results of the fluid conductivity analysis presented in Table 5. The elapsed time of pumping, t, is taken as the time between the start of pumping at 6:50 a.m. on February 20, 1985, and the time of the last fluid conductivity log used in the analysis of inflows at 9:24 a.m. on February 22, 1985. The total elapsed time is therefore 50.5 hours or 1.82×10^5 sec. It bears noting that the times t_i, recorded in Table 5, indi-

cate the estimated start of inflow of formation water from the individual water-producing zones into the borehole and do not have to correspond with the start of pumping. Caliper logs indicate only slight changes in borehole diameter within the section under study. Well bore radius r_{w_i} is thus assumed constant, with r_{w_i} = 0.07 m. If fractured rock is conceptualized as an equivalent porous medium, storativity may be expressed as

$$S = S_s m = \rho g(a + nb)m \tag{22}$$

where ρ is formation fluid density, g is the gravitational constant, a is rock compressibility, n is porosity, and b is formation fluid compressibility. Of these, only the rock compressibility and formation porosity can vary substantially.

Based on a literature review, Belanger et al. (1988) have considered as a best guess porosity of 0.005 and rock compressibility of 2.0×10^{-11}/Pa for this site. This results in a "base-case" specific storativity of 2.0×10^{-7}/m. This value was varied by Belanger et al. (1988) in a sensitivity analysis to determine the specific storativity that best fits the observed pressures during hydraulic testing of the Leuggern borehole. In the hydraulic tests that correspond to the test intervals of interest with respect to the present comparison with fluid electric conductivity logging (see Table 6), the specific storativity used by Belanger et al. (1988) was generally the base-case value of 2.2×10^{-7}/m. The exception to this occurred in interval 918.4H, where a specific storativity of 2.0×10^{-5}/m was used, and in interval 1034.2S, where a value of 2.0×10^{-6}/m was used. For all test intervals, Belanger et al. (1988) assumed further that the thickness m of the water-producing zone is equivalent to the length of the packed-off test section. Thus m varied between 12.0 and 25.0 m for all hydraulic packer tests analyzed by Belanger et al. (1988) in the section under study.

Hence for the sake of comparison, the same base-case specific storativity of 2.2×10^{-7}/m, as used by Belanger et al. (1988) in the analysis of the packer tests, is used in the analysis of the fluid conductivity logging. However, to demonstrate the minor sensitivity of transmissivity values determined from fluid conductivity logging to the selected storativity as well as to the the thickness of the water producing zone, several test cases (Case A to E) are presented in Table 7,

Table 6. Comparison of transmissivities derived from fluid logging and conventional packer hydraulic testing

Test Name	Packer Hydraulic Testing Interval				Fluid Logging (Case C)	
	Bottom (m)	Top (m)	Length (m)	T (10^{-9} m^2/s)	Peak No.	T (10^{-9} m^2/s)
1437.0H	1449.5	1424.5	25.0	0.25	1	3.5
1433.4D	1439.4	1427.4	12.0	1.2		
1304.2S	1315.1	1293.4	21.7	0.65	2	3.2
1215.0H	1227.6	1202.6	25.0	1.3	3	2.9
1203.2D	1227.1	1179.3	47.8	4.8	3+4+5	7.6
1192.5D	1208.8	1176.2	32.6	3.3	4+5	4.7
1082.9H	1095.4	1070.4	25.0	0.75	6	0.95
1046.0H	1058.5	1033.5	25.0	0.25	7	3.2
923.0D	929.7	916.2	13.5	9.5	8	4.1
918.4H	930.9	905.9	25.0	0.75		
912.5S	919.2	905.9	13.3	0.53		
850.0S	859.5	840.5	19.0	570	9	120
847.0D	859.5	834.5	25.0	500		
837.8H	850.3	825.3	25.0	750		

S: Single packer test;
D: Double packer tests;
H: Hydraulic reconnaissance test

where S_{s_i} varies from 2.2×10^{-7}/m to 2.0×10^{-5}/m and m varies between 0.1 m and 10 m.

Table 7 clearly demonstrates the low sensitivity of transmissivity to the storage coefficient and thickness of the water-producing zone. Two orders of magnitude deviation of S_s and m from the base-case values results in only a factor of 2 to 3 change in transmissivity. This factor is negligible, given all the other uncertainties introduced by conceptualizing heterogeneous fractured rock as a homogeneous equivalent porous medium.

As can be seen from Table 7, transmissivities determined from fluid conductivity logging range from approximately 2.0×10^{-7} m^2/s to 5.0×10^{-10} m^2/s. The measurement range of more than two orders of magnitude demonstrates the very high sensitivity of the method and the extremely low transmissivities that can still be detected.

Table 7. Transmissivities derived from fluid conductivity logging for test cases A through E. Base case is C.

Peak No.	Depth (m)	q_i ($10^{-6}m^3/s$)	Transmissivity ($10^{-9}m^2/s$) Case A	Case B	Case C	Case D	Case E
1	1440	0.65	4.9	4.2	3.5	2.7	1.9
2	1300	0.60	4.5	3.9	3.2	2.5	1.8
3	1215	0.55	4.1	3.5	2.9	2.3	1.6
4	1200	0.25	1.8	1.5	1.2	0.92	0.62
5	1188	0.65	4.9	4.2	3.5	2.7	1.9
6	1085	0.20	1.4	1.2	0.95	0.72	0.47
7	1048	0.60	4.5	3.9	3.2	2.5	1.8
8	918	0.75	5.7	4.9	4.1	3.2	2.3
9	843	17.	160	140	120	99	79

Case A: $S_s = 2.2\times10^{-7}$/m; m = 0.1m
Case B: $S_s = 2.2\times10^{-7}$/m; m = 1.0m
Case C: $S_s = 2.2\times10^{-7}$/m; m = 10.0m (base case)
Case D: $S_s = 2.0\times10^{-6}$/m; m = 10.0m
Case E: $S_s = 2.0\times10^{-5}$/m; m = 10.0m

Comparison of Transmissivities Derived from Fluid Conductivity Logging and Conventional Hydraulic Testing

To validate the transmissivity values derived from fluid conductivity logging, a comparison is made below with the transmissivities determined independently from packer hydraulic testing in the Leuggern borehole.

A large number of hydraulic tests were conducted during drilling and after completion of the Leuggern borehole. All of the tests were configured in terms of either single packer tests or double packer tests, (Leech et al., 1984). Single packer tests were typically used during drilling to isolate the bottom section of the borehole with the aim of (i) determining formation hydraulic head, (ii) collecting water samples, and (iii) estimating hydraulic conductivity. Double packer tests use an upper and lower packer to isolate specific intervals within the borehole. These tests were typically completed after drilling in order to assess or reassess intervals of importance. Their primary use was to collect water samples and to conduct pump tests. Hydrogeological reconnaissance tests (so-called H-log tests) were conducted in double packer configuration to test the borehole continuously at 12.5- or 25-m intervals.

The three test types (single packer, double packer, and H-log tests) typically used one or more of the following hydraulic test methodologies at each test interval: (i) slug tests, (ii) pulse tests, (iii) drill-stem tests, and (iv) pump tests. A detailed discussion of the tests and the interpretation methods applied in the NAGRA boreholes is provided by Grisak et al. (1985). For the analysis of the tests, the numerical borehole simulator GTFM (Pickens et al., 1987) was used in combination with trial-and-error techniques to estimate best-guess hydraulic conductivities. The model is based on the commonly conceptualized equivalent-porous-medium assumption, i.e., each test interval is treated as a homogeneous single confined aquifer. GTFM allowed borehole pressure history and isothermal and nonisothermal fluid conditions in the borehole to be incorporated in the analysis. Analysis methods and results are described in detail in Belanger et al. (1988).

All the 14 hydraulic tests that cover the depth locations identified by fluid logging as being inflow zones were drawn from Belanger et al. (1988). Based on the reported average hydraulic conductivity and interval length, a transmissivity was calculated for each test interval. Table 6 shows a comparison between the transmissivities derived from packer testing and from fluid logging.

As can be seen from the table, in some locations there are up to three packer tests, e.g., tests 850.0S, 847.0D, and 837.8H, covering a specific inflow point (peak No. 9), whereas at other locations, there are up to three peaks, e.g., peaks 3+4+5, within the interval of only one packer test (test 1203.2D). In the latter case, single peak transmissivities were added together in order to derive the test interval transmissivity.

The main conclusion from the comparison is that fluid conductivity logging leads to transmissivities that are in very good agreement with conventional packer hydraulic testing. The transmissivities derived from fluid conductivity logging are generally within half an order of magnitude of those derived from conventional packer testing. This is remarkable, considering that in the fluid conductivity logging method inflows from fractures are estimated completely independent from the packer tests by applying a borehole fluid advection-dispersion model to observations of electric conductivity of the borehole fluid.

Let us now focus on the three intervals in Table 6 where a discrepancy of an order of magnitude appears to exist. From the borehole sections with multiple, overlapping packer tests straddling the single inflow zones 1 and 8, it is interesting to note that differences of up to one order of magnitude and more in transmissivity do occur among the individual packer tests. The double packer tests in the above intervals exhibit significantly higher transmissivities than the single packer tests and H-log tests. Belanger et al. (1988) attribute this characteristic to the possible existence of lower hydraulic conductivity zones near the borehole. Short-term tests like the single packer and H-log tests would be highly influenced from such zones, whereas the longer-duration double packer tests (conducted primarily for water sampling) are more representative of higher hydraulic conductivities farther away from the borehole. Therefore, for the comparison of

the packer test results with the results of fluid logging, the longer-duration double packer tests, with a test duration similar to the duration of the fluid logging tests, are deemed more representative. Transmissivities derived from double packer tests at zones 1 and 8 are in close agreement with the results of fluid electric conductivity logging. At inflow zone 7, the difference between the H-log test and the fluid conductivity logging is about one order of magnitude. The H-log test, however, was of relatively short duration compared to fluid logging, and we cannot rule out the possibility that the H-log underestimates the longer-duration transmissivity of this zone.

On the basis of the above remarks, the overall agreement between the transmissivities derived from the different methods is remarkable.

Comparison with Results of Hydrochemical Sampling

Water samples were collected in the Leuggern borehole at various depths to determine the chemical composition and the age of the deep groundwaters. To facilitate a proper sample analysis, tracer-marked deionized water was used during drilling of the crystalline section of the borehole. The tracers added to the drilling fluid were Na-fluorescein (Uranine) and meta-trifluoromethylbenzoic acid (m-TFMBA). The tracers served to indicate the degree of contamination of the sampled formation water by drilling fluids. Water was generally produced from the formation prior to taking a final sample until the reduction in the tracer level indicated a negligible residual contamination of the formation water, on the order of 1-2%. In a few cases, where tracer concentrations higher than 2% were found in the final sample, uranine and m-TFMBA concentrations were used to determine true formation water composition by extrapolation from the contaminated samples. A detailed description of the sampling methods and hydrochemical analyses of the waters collected in the Leuggern borehole is given in Wittwer (1986).

From Wittwer (1986), four zones can be identified where formation water composition was analyzed within the section of the Leuggern borehole that was subsequently studied with fluid conductivity logging. Information about the chemical composition of the formation water from these zones is summarized in Table 8. The zones are identical with the double packer test intervals indicated in Table 6. No analysis was conducted on the water from zone 1192.5D, for

Table 8. Chemical composition and electric conductivity of formation water from four test sections

Test Section	Cations					Anions				Dissolved Solids mg/L	Total Conductivity µS/cm*
	Na^+ mg/L	K^+ mg/L	Mg^{2+} mg/L	Ca^{2+} mg/L	Total mg/L	Cl^- mg/L	SO_4^{2-} mg/L	HCO_3^- mg/L	Total mg/L		
1433.4D	468	10	1	13	497	422	278	195	915	>1453	>2030†
1203.2D	310	6	0	6	323	131	269	217	915	974	1290
923.0D	1108	13	2	424	1561	203	3057	73	3336	4988	4965
847.0D	334	8	0	16	360	122	361	217	727	1128	1437§

*Minimal values

†Formation water properties estimated by extrapolation from a water sample with 3-6% contamination

§Normalized to 20°C

which, according to Wittwer (1986), the contamination of the sample remained too high. Caution is recommended with sample 1433.4D, since irregular behavior of tracer concentrations and electric conductivity during the cleaning phase indicate that some contamination with variable-composition borehole fluid may have remained in the formation. It is thus suggested by Wittwer (1986) that the water sample from test section 1433.4D represents a lower limit for total dissolved solids and formation water electric conductivity.

In Table 8, the concentrations of the major cations and anions are presented together with total dissolved solids and electric conductivity. The small differences between the summed concentrations of major cations and anions and the total concentrations of cations and anions, on the order of a few mg/L, is caused by a series of minor constituents not displayed in the table. For details, the interested reader is referred to Wittwer (1986).

The data presented in Table 8 make it clear that the formation waters from the various test sections are chemically different and are not pure NaCl solution, as we have assumed in establishing a relation between electric conductivity and electrolyte concentration (equation 2). The water from test section 1433.4D is of the Na-Cl-SO_4-HCO_3 type, the waters from test sections 1203.2D and 847.0D are both of the Na-SO_4–HCO_3-Cl type, and the water from test section 923.0D can be characterized as of the Na-Ca-SO_4 type. The observed differences in chemical composition of the formation water do not, however, prevent the electrolyte concentration or its measure, electric conductivity, to be utilized to quantify the volumetric flow of water. This is also supported by the observed close relation between total dissolved solids and electric conductivity.

Table 9 shows a comparison of formation water electric conductivity determined from the water sampling and electric conductivity logging. In addition, equivalent NaCl concentration of the formation water is calculated from the formation water electric conductivity by dividing electric conductivity by the factor $\alpha = 1870$ (µS/cm) $\cdot$ (m^3/kg) used in equation (2).

Table 9. Comparison of formation water electric conductivity (at 20°C equivalent) derived from fluid conductivity logging and from water sampling

Test Section	Water Sampling Electric Conductivity µS/cm	Peak No.	Electric Conductivity eq. NaCl Concentration mg/L	Logging Electric Conductivity µS/cm
1433.4D	>2030	1	500	940
1203.2D	1290	3+4+5	430	800
923.0D	4965	8	5,500	10,000
847.0D	1437	9	950	1,800

The main conclusion to be drawn from Table 9 is that formation water electric conductivities estimated from fluid conductivity logging are generally in good agreement, within a factor of 2, with electric conductivities observed in the samples of the formation water. This is especially remarkable if one considers that the estimates of formation water conductivity from fluid logging were made based on an incomplete buildup of the electrolyte concentration in the borehole fluid.

Special attention should be given to the fact that the formation water electric conductivity of peak 8 is predicted from fluid conductivity logging to be 5-10 times higher than that of the other peaks. This is again closely confirmed by the water samples.

Conclusion and Discussion

In this paper we first discuss the procedure and physical processes associated with a time series of fluid conductivity logs in a borehole intersected by a number of flowing fractures. Simple formulas to evaluate some of the relevant parameters are described and their uses demonstrated. Then numerical matching of the data to obtain the remaining parameters is shown. The results are not sensitive to borehole radius variations and the method may be able to measure small inflow rates. From Table 5, it appears that flow rate as low as $0.2 \times 10^{-6} m^3/s$, or 0.01 L/min, can be measured. This may prove to be a useful technique to complement existing flowmeter or temperature log methods.

The flow rates from each fracture obtained by the fluid conductivity logging method are used together with other information to estimate fracture transmissivities for the Leuggern

borehole in Switzerland. The method and results were validated against transmissivity obtained independently by conventional hydraulic testing using packers. The agreement is remarkable. The method and results of salinities of fracture fluids are further validated against independent results of chemical analysis of fluid samples taken from various depths in the Leuggern borehole. They are in general good agreement. In particular the above-average salinity at peak 8 is confirmed by the water sampling analysis results.

To conclude this paper, we briefly discuss some practical aspects as well as some of the limitations and advantages of the proposed borehole fluid electric-conductivity logging method.

Obviously for a successful test using this method, it is necessary to create inflow from the formation into the borehole, which requires the lowering of the pressure in the borehole fluid column below the formation pressure. Water from the borehole could be intermittently pumped, although the analysis can be easier if constant-rate pumping is conducted. Further, a significant contrast in electric conductivity between the formation water and the borehole fluid is required. In the case of high conductivity of the formation water, a low conductivity fluid should be applied in the borehole and vice versa.

Like any experimental technique, electric conductivity logging is subject to detection limits. The lower detection limit for inflowing formation water is determined by the ability to properly identify and quantify electric conductivity changes caused by the inflow. This is controlled by processes that dissipate the electric conductivity contrast between the formation water and the borehole fluid. Two processes are important: (i) dispersion in the borehole, which tends to smear out the electric conductivity peaks; and (ii) dilution of the inflowing formation water by the existing flow within the borehole, which limits the maximum conductivity values of these peaks. In the Leuggern borehole it was possible to detect and quantify single inflows down to some 5 to 10 mL/min corresponding to fracture transmissivities as low as 10^{-9} to 10^{-10} m^2/s. It is the dilution of the water flowing into the borehole that causes the most severe limitation. Because the inflow is a fraction of the flow in the borehole, the detection limit increases toward the pump, since the flow rate in the borehole, being the sum of all the inflows, also increases toward the pump. How-

ever, dilution can be controlled to some extent by isolating (for example, with a packer) a higher-producing part of the borehole and testing the remaining section above it. This procedure was successfully applied in the Leuggern borehole.

An upper detection limit, on the other hand, is also created by high flows into the borehole. In this case, the borehole fluid is replaced by formation water at a speed that is too fast for properly logging the growth rate of the peaks. This is indicated in the Leuggern borehole near the top of the logged section, where conductivity saturation had already been reached before the first logging run took place. Maximum flow rates in the borehole can to some extent be controlled by adjusting the pump rate. However, in the case of large differences in the formation head along the borehole, natural flow without pumping might be too high. If this is the case, application of a borehole spinner or packer flowmeter seems more appropriate.

Based on the experience NAGRA gained while conducting the feasibility studies and safety analyses for Project Gewahr 1985, which involved an extensive regional investigation program in deep boreholes drilled in sedimentary-covered crystalline rocks in northern Switzerland (NAGRA, 1985; Thury and Gautschi, 1986; NAGRA, 1988), fluid logging techniques proved to have several advantages and may play a significant part in a well-planned borehole testing program. First, they allow an identification of the locations of water-conducting fractures or groups of fractures in a borehole. This is very important for subsequent core investigations aiming at a detailed geological and geochemical description of preferential flow paths through the rock mass. Second, fluid logging may be used to derive the hydraulic or flow properties, like transmissivity, of these identified water-conducting features. Such a technique would be a cost-effective alternative to the conventional hydraulic single and double packer testing. Even if conventional hydraulic testing were not completely eliminated, fluid logging could effectively be applied as a screening tool prior to hydraulic testing and water sampling. In conclusion, even though there are limitations to the proposed method, the advantages discussed above render the method quite promising.

References

Bean, H. S. (1971), *Fluid Meters: Their Theory and Application,* American Association of Mechanical Engineers, 6th Edition, New York.

Belanger, D. W., Freeze, G. A., Lolcama, J. L. and Pickens, J. F. (1988), Interpretation of Hydraulic Testing in Crystalline Rock at the Leuggern Borehole. Nagra Technical Report NTB 87-19, Nagra, Baden, Switzerland, December 1988.

Bodvarsson, G. S. (1982), Mathematical Modeling of the Behavior of Geothermal Systems under Exploitation, Ph.D. Thesis, University of California at Berkeley, Department of Materials Sciences and Mineral Engineering.

Cooper, H. H., Jr. and Jacob, C. E. (1946). A Generalized Graphical Method for Evaluating Formation Constants and Summarizing Well-Field History. *Transactions American Geophysical Union, 27.* pp. 526 - 534.

Grisak, G. E., Pickens, J. F., Belanger, D. W. and Avis, J. D. (1985). Hydrogeologic Testing of Crystalline Rocks During the NAGRA Deep Drilling Program. Nagra Technical Report NTB 85-08, Nagra, Baden, Switzerland, January 1985.

Hale, F. V. and Tsang, C. F. (1988). A Code to Compute Borehole Fluid Conductivity Profiles with Multiple Feed Points, NDC-2, LBL-24928, Lawrence Berkeley Laboratory, Berkeley, CA.

Hess, A. E. (1986), Identifying Hydraulically-Conductive Fractures with a Low Velocity Borehole Flowmeter, *Canadian Geotech. Journal, 23* (1), 69-78.

Hufschmied, P. (1983), Ermittlung der Durchlässigkeit von Lockergesteins - Grundwasserleitern, eine vergleichende Untersuchung verschiedener Feldmethoden, Diss. No. 7397, ETH Zurich, Switzerland.

Jacob, C. E. (1940). On the Flow of Water in an Elastic Artesian Aquifer, *EOS, Transactions, American Geophysical Union, 21,* 574 - 586.

Leech, R. E. J., Kennedy, K. G. and Gevaert, D. (1984), Sondierbohrung Böttstein, Hydrogeologic Testing of Crystalline Rocks. Nagra Technical Report NTB 85-09, Nagra, Baden, Switzerland, December 1984.

NAGRA (1985), Project Gewähr 1985, Nuclear Waste Management in Switzerland: Feasibility Studies and Safety Analyses, NAGRA Project Report NGB 85-09, Nagra, Baden Switzerland, June 1985.

NAGRA (1988), Fluid-Logging der Sondierbohrungen Bottstein, Weiach, Riniken, Schafisheim, Kaisten and Leuggern, Temperature, Leitfähigkeits and Spinner Flowmeter Messungen, NAGRA Technical Report NTB 85-10, Nagra, Baden, Switzerland, October 1988.

Omega (1987), *Complete Flow and Level Measurement Handbook and Encyclopedia,* Omega Engineering, Inc., Stamford, Connecticut.

Paillet, F. L., Hess, A. E., Cheng, C. H. and Hardin, E., (1987), Characterization of Fracture Permeability with High Resolution Vertical Flow Measurements during Borehole Pumping, *Ground Water, 25* (1) 28-40.

Pickens, J. F., Grisak, G. E., Avis, J. D., Belanger, D. W. and Thury, M. (1987), Analysis and Interpretation of Borehole Hydraulic Tests in Deep Boreholes: Principles, Model Development, and Applications. *Water Resour. Res., 23,* (7) 1341-1375.

Shedlovsky, T. and Shedlovsky, L. (1971), "Conductometry," *Techniques of Chemistry,* (Arnold Weissberger and Bryant W. Rossiter, eds.), Vol. 1. Physical Methods of Chemistry, Part IIa, Electrochemical Methods, John Wiley & Sons, Inc., New York.

Theis, C. V. (1935), The Relationship Between the Lowering of the Piezometric Surface and the Rate and Duration of Discharge of a Well Using Groundwater Storage. *Transactions, American Geophysical Union, 16,* 519-524.

Thury, M. and Gautschi, A. (1986), Testing Programme in Deep Boreholes Drilled in Sediment-Covered Crystalline Rocks in Northern Switzerland, *Proceedings of the 2nd International Conference on Radioactive Waste Management,* Canadian Nuclear Society, September 7-11, 1986, Winnipeg, Manitoba, Canada.

Tsang, C. F. (1985), Lessons Learned in the Verification and Validation Studies of a Coupled Heat and Fluid Flow Code, Invited Paper, Proceedings of Symposium on Groundwater Flow and Transport Modeling for Performance Assessment of Deep Geologic Disposal of Radioactive Waste: A Critical Evaluation of the State of the Art, May 20-21, 1985, Albuquerque, New Mexico.

Tsang, C. F. and Doughty, C. (1985), Detailed Validation of a Liquid and Heat Flow Code Against Field Performance, Proceedings of the Eighth SPE Symposium on Reservoir Simulation, February 10-13, 1985, Dallas, Texas, organized by Society of Petroleum Engineers, Richardson, Texas.

Wittwer, C. (1986), Probenahme und Chemische Analysen von Grundwassern aus den Sondierbohrungen. Sondierbohrungen Bottstein, Weiach, Riniken, Schafisheim, Kaisten, Leuggern. Nagra Technical Report NTB 85-49, Nagra, Baden, Switzerland, October 1986.

INFORMATION RESOURCES DEPARTMENT
LAWRENCE BERKELEY LABORATORY
UNIVERSITY OF CALIFORNIA
BERKELEY, CALIFORNIA 94720